Kinetic studies of CO_2 methanation over a Ni/γ-Al_2O_3 catalyst using a batch reactor

Jin Yang Lim[1], J. McGregor[2], A. J. Sederman[1], J. S. Dennis[1]

[1] Department of Chemical Engineering and Biotechnology, University of Cambridge, Cambridge CB2 3RA, United Kingdom.

[2] Department of Chemical and Biological Engineering, The University of Sheffield, Sir Robert Hadfield Building, Portobello Street, Sheffield, S1 3JD, United Kingdom.

Abstract

The methanation of CO_2 was investigated over a wide range of partial pressures of products and reactants using a gradientless, spinning-basket reactor operated in batch mode. The rate and selectivity of CO_2 methanation, using a 12 wt% Ni/γ-Al_2O_3 catalyst, were explored at temperatures 453 – 483 K and pressures up to 20 bar. The rate was found to increase with increasing partial pressures of H_2 and CO_2 when the partial pressures of these reactants were low; however, the rate of reaction was found to be insensitive to changes in the partial pressures of H_2 and CO_2 when their partial pressures were high. A convenient method of determining the effect of H_2O on the rate of reaction was also developed using the batch reactor and the inhibitory effect of H_2O on CO_2 methanation was quantified. The kinetic measurements were compared with a mathematical model of the reactor, in which different kinetic expressions were explored. The kinetics of the reaction were found to be consistent with a mechanism in which adsorbed CO_2 dissociated to adsorbed CO and O on the surface of the catalyst with the rate-limiting step being the subsequent dissociation of adsorbed CO.

Keywords: methanation of CO2; kinetic measurements; nickel/alumina catalyst; modelling

1. Introduction

In response to anthropogenic climate change, it is expected that the number of carbon-capture schemes is expected to increase. As a result, the increased availability of CO_2 is likely to drive its cost down, so that heterogeneous catalysis could be used to convert CO_2 to various chemicals such as methane, methanol, formic acid and dimethyl carbonate (Aresta *et al*., 2007; Ma *et al.*, 2009). Of course, CO_2 is thermodynamically very stable and the main challenge in converting it to other organic products is providing the free energy needed. In particular, the production of methane by reacting CO_2 with H_2 (CO_2 methanation) has the potential for producing synthetic natural gas (SNG), which could be distributed using the existing infrastructure for the distribution of natural gas (Kopyscinski, 2010). Furthermore, the study of the chemistry of CO_2 in methanation could provide insights into related reactions, such as the Fischer-Tropsch synthesis and CO methanation.

Various transition metals are active in catalysing the methanation of CO_2, *i.e.*

$$CO_2 + 4H_2 \rightarrow CH_4 + 2H_2O\,. \qquad \text{(R1)}$$

A number of previous investigations of CO_2 methanation, particularly over Co and Fe catalysts, have arisen as a result of research designed to study, primarily, the conversion of CO_2 to long-chain paraffins or olefins *via* Fischer-Tropsch synthesis, where methane is inevitably produced as a major product (Zhang *et al.*, 2002; Riedel *et al.*, 2003). Ruthenium-based catalysts have received much attention, owing to their high reactivity and selectivity for the methanation of CO_2 (Kowalczyk *et al.*, 2008; Zağli and Falconer, 1981; Marwood *et al.*, 1997). Supported Rh catalysts have been investigated because of their ability to catalyse the methanation of CO_2 at very low temperatures, *viz.* below 100°C (Jacquemin *et al.*, 2010). The field has been reviewed recently by Gao *et al*. (2015). Mixed Ni/Pt or Ni/Pd catalysts have also received attention (Porosoff and Chen, 2013) in batch reactor studies, with most studies building on the seminal work and mechanistic modelling of Xu & Froment (1989), which examined steam-methane reforming, methanation and water-gas shift kinetics.

Although catalysts based on either Ru or Rh have been shown to be more active than nickel-based catalysts, the cost of such metals is prohibitive for their widespread use in industry. Nickel-based catalysts remain the most widely-studied materials owing to the abundance of Ni and its low cost. For the methanation of CO_2, nickel catalysts are often active at temperatures above 150°C, but the exact reaction mechanism is still subject to debate. The key question is whether the reaction occurs (i) by the dissociative adsorption of

CO_2 to form CO and O on the surface of the catalyst (Falconer and Zağli, 1980; Weatherbee and Bartholomew, 1981; Fujita *et al*., 1991; Fujita *et al.*, 1993), or (ii) by the conversion of CO_2 to methane *via* carbonate or formate intermediates which do not involve CO, as suggested by Aldana *et al.* (2013).

It has become increasingly clear that the reaction pathway depends on the nature of the support. Whilst a number of studies have been performed on various types of supported nickel catalysts by characterising the structure and phases of the synthesised material (Aksoylu *et al.*, 1996; Liu *et al.*, 2013; Du *et al.*, 2007), only a few investigations have performed rigorous kinetic studies on the rate and selectivity of CO_2 methanation at different temperatures, overall pressures and partial pressures of reactants and products. Given that the mechanistic pathways could differ for different catalysts, it is not unreasonable to expect that rate expressions differ for different catalysts, with important implications in reactor operation and design in industry.

The primary objective of this work was to investigate the kinetics of the methanation of CO_2 over nickel supported on Al_2O_3 over a wide range of partial pressures of reactants and products, and at relatively low temperatures < 210°C, to determine if the kinetics and rate expressions were consistent with previously-proposed theories. Only a few previous studies have proposed rate expressions for the methanation of CO_2 (*e.g.* Weatherbee and Bartholomew, 1982; van Herwijnen *et al.*, 1973). The conclusions of these researchers were based on experiments which were performed on continuous, flow reactors. One way of validating the rate expressions is to examine their applicability over a wide range of partial pressures of reactants and products, conveniently achieved by conducting the reaction in a batch reactor. Here, we have undertaken a study of the kinetics of the methanation of CO_2 in a gradientless, spinning-basket reactor operating in batch.

2. Experimental

2.1. Catalyst and characterisation

A 12 wt% Ni catalyst was prepared by the incipient wetness impregnation of pellets of γ-alumina (Saint Gobain – SA 62125, 3 mm dia. spheres) using $Ni(NO_3)_2.6H_2O$ as the precursor salt (Sigma-Aldrich). The pore volume of the support was reported to be 0.64 ml/g, experimentally verified by adding de-ionised (DI) water dropwise to the pellets until they had

a glistening appearance, indicating that the pores were fully filled, and measuring the total volume of water used.

The impregnated catalyst was dried for 24 hours at 120°C in a hotbox oven prior to calcination at 450°C for 4 hours in 150 ml/min (as measured at 293 K and 1 bara) of air in a tubular quartz reactor and heated by a furnace at atmospheric pressure. Subsequently, H_2 was introduced at a flowrate of 100 ml/min (as measured at 293 K and 1 bara) at 700°C for 6 hours to reduce the calcined catalyst to metallic Ni. A temperature of 700°C was used to ensure that all available nickel oxide could be reduced to metallic nickel. The reduced catalyst was passivated in a mixture of 5 vol% O_2 and N_2 at 25°C, before being transferred to a Carberry spinning-basket reactor (described below) to investigate different reactions. Prior to each experiment in the Carberry reactor, the passivated catalyst was reduced *in situ* by hydrogen at 250°C overnight, for approximately 12 hours.

The catalyst was characterised by a BET surface area of 155 $m^2\ g^{-1}$ and BJH pore volume of 0.46 $cm^3\ g^{-1}$.A dispersion of 12 % was obtained, based on pulse H_2 chemisorption experiments. Temperature programmed reduction was performed in a Hiden CATLAB microreactor, where the composition of the off-gas was measured by a mass spectrometer (Hiden QIC-20). The evolution of H_2O from the reduction of NiO to Ni by H_2 was used to study the reducibility of the different samples. The profiles of temperature programmed reduction (TPR) of the different samples are illustrated in Figure 1. In general, the investigations monitoring the off-gas of the reactor were consistent with the observations from a thermogravimetric analyser (TGA) (Mettler Toledo TGA/DSC 1 STARe system). For the calcined NiO/Al_2O_3 and the passivated Ni/Al_2O_3, two main H_2O peaks were observed, one at 280°C and another at 570°C. The H_2O peak at 180°C was attributed to evolution of moisture on the surface of the samples because no corresponding consumption of H_2 was observed (not shown). Figure 1 also shows that the passivated Ni/Al_2O_3 has significantly less NiO reduced at temperatures above 450°C, implying that the procedure for reduction at 700°C in the synthesis process had converted most of this NiO to metallic Ni. The passivation process appeared to have given rise to the NiO peak at 280°C. The passivated Ni/Al_2O_3 catalyst had to be reduced *in situ* in the Carberry reactor before catalytic reactions could be performed. The efficacy of this protocol was confirmed through temperature programmed reduction studies, the results of which are shown in Figure 1, where it is clear that negligible amounts of the 'low temperature' NiO remained after an isothermal reduction at 250°C for 9 hours.

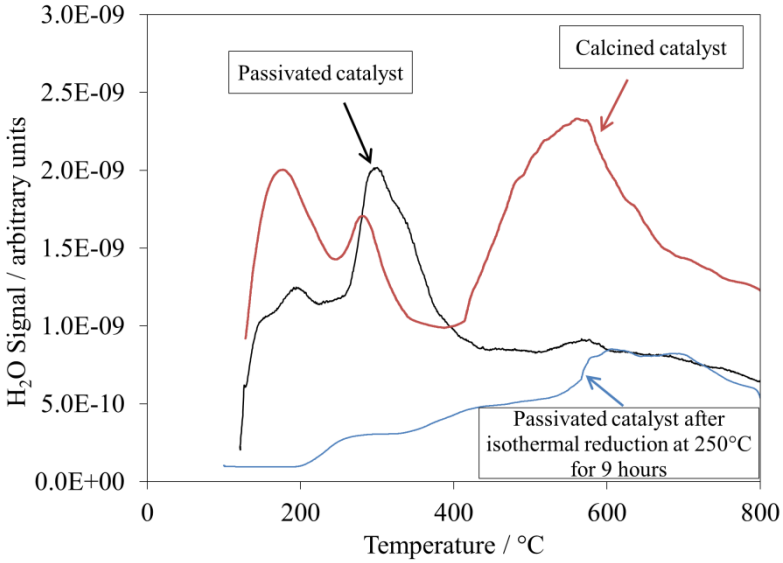

Figure 1. H_2O signal versus temperature for a temperature programmed reduction on calcined NiO/Al_2O_3, passivated Ni/Al_2O_3 and passivated Ni/Al_2O_3 which was pre-treated with an isothermal reduction at 250°C for 9 hours.

The CATLAB apparatus was also used to perform temperature-programmed desorption of the spent catalyst following the reaction studies in the batch reactor: this will be elaborated on in Section 2.2. *In-situ* diffuse reflectance infrared spectroscopy (DRIFTS) was also performed on 50 mg of the catalyst in a flow of CO_2 and H_2 at 463 K under atmospheric pressure (Praying Mantis, Harrick Scientific). For each measurement, a series of 128 scans was performed with spectral resolution of 2 cm^{-1} and a final spectrum was obtained by averaging the 128 scans. For every measurement a background spectrum was collected and automatically subtracted from the sample spectrum.

2.2. Studies of methanation in a batch reactor

A spinning-basket reactor was used to study the kinetics of CO_2 methanation, using the 12 wt% $Ni/\gamma\text{-}Al_2O_3$ catalyst. A schematic diagram of the experimental arrangement is shown in Figure 2. The reactor, made of 316 stainless steel (Carberry reactor, i.d. 75 mm, 401A-8801, Autoclave Engineers, USA), had a maximum operating temperature and pressure of, respectively, 250°C and 50 bar. The volume of the reactor was reported by the manufacturers to be 2.95×10^{-4} m^3, which was confirmed by measuring the drop in the pressure of the sealed reactor after the removal, by the use of a syringe, of a known volume of gas at room temperature and elevated pressure. The reactor was equipped with a removable basket, which

had a mesh size of 1.3 mm, connected to a rotating shaft. The baffles and impeller helped to ensure that the reactor volume was gradientless in terms of heat and mass transfer external to the catalyst particles. All connections in the apparatus, including tubes and fittings, were made of 316 stainless steel. The reactor was heated externally by two band heaters (Me5J1JP1, Watlow) with a total power output of 1 kW, capable of controlling the temperature of the reactor to a precision of ± 0.1 K when steady-state was achieved.

In a typical experiment, the basket in the reactor was first loaded with a known amount of catalyst and packed with a non-porous inert material, glass beads (1.4 mm diam.), such that about 5.0 g of catalyst pellets were mixed with an equal mass of glass beads in the basket. The reactor was sealed and the vacuum pump was turned on, with the valve to the vent closed, to evacuate the gaseous content of the reactor. The reactor was heated to 250°C and the catalyst was then subjected to a flow through the reactor of 100 ml/min (at room temperature and pressure) of H_2 with a stirring at 1.7 Hz for 12 hours at 1 bar. The flow of H_2 was controlled by a rotameter and a needle valve. Following the reduction in H_2, the reactor was evacuated once again using the vacuum pump and the internal temperature of the reactor brought to the desired reaction temperature. The rate of the reaction of interest was studied in batch by bringing the reactor to a desired initial pressure and composition, using gas supplied from the cylinders connected to the reactor. During this period, the three-way valve was used to isolate the rotameter for hydrogen, shown in Figure 2, in order to prevent its exposure to pressures above atmospheric pressure. Gas cylinders with pre-mixed gases were normally used and the reactor could be brought to the desired pressure using one cylinder only. The initial total pressure of the reactor was typically 10 – 20 bar. In order to raise the pressure of the reactor, the pressure regulator on the gas cylinder of interest was first adjusted to about 2 bar higher than the desired pressure of the reactor. This was followed by fully opening the needle valve at the inlet of the reactor and then opening the plug valve, raising the pressure of the reactor. While the pressure was being raised, the flow of the gas from the cylinder into the reactor was controlled by progressively closing the needle valve. As the pressure approached the desired value, the needle valve would be almost fully closed. The plug valve of the corresponding line was closed when the reactor reached the desired pressure. With this procedure, the final pressure of the reactor could be consistently achieved to a precision of ± 0.1 bar, which was approximately the precision of pressure gauge PG1. The accuracy of the measurement of pressure was confirmed by good agreement between the readings of the two pressure gauges, PG1 and PG2. If the desired starting composition in the reactor was different from that in any gas cylinder, different gases were introduced into the reactor in stages. This

was achieved by monitoring the total pressure, recorded by the two pressure gauges, of the reactor after successive additions of gas from the various cylinders. A stirrer speed of 9.2 Hz was always used. The entire process of bringing the reactor to the desired pressure and starting the stirrer after the introduction of the gases typically took 10 – 15 s.

After the reactive gases were introduced, the changes in the composition of the reactor volume were measured over time. This was performed by taking volumes of 4 ± 0.2 ml (at atmospheric temperature and pressure) from the reactor using a gas-tight sampling syringe. Prior to the removal of the sample by the syringe, the gaseous contents of the lines after needle valve 'A' in Figure 2 were evacuated by the vacuum pump. The plug valves 'B' and 'C' were then closed and the volume enclosed by valves 'A', 'B' and 'C' was brought to 3 bar using the needle valve 'A' and monitored by pressure gauge PG3. The gas collected here was purged through the vent and the space evacuated once again before the actual sample was taken. The latter operation was performed as a precaution to minimise the effect of dead volume in the section of the reactor which might not have mixed well with the bulk phase of the reactor volume, *i.e.* within the connection through the walls of the reactor to the outlet at valve 'A'. This procedure ensured that the composition of the sample of gas obtained from the reactor was representative of the contents of the bulk phase of the reactor volume. Only about 6 – 10 samples were taken for each experiment so as to minimise the errors incurred from the removal of gaseous contents from the reactor. The composition of the sample was analysed using off-line gas chromatography (Agilent 7890 GC Extended Refinery Gas Analysis) by passing the sample in the syringe through the sampling loop in the gas-chromatograph. The sampling loop in the gas chromatograph was evacuated using a vacuum pump before the gaseous contents of the syringe were introduced.

The composition of the gas given by off-line gas chromatography would only be equal to that in the bulk phase of the reactor if all species in the gas phase were above their dew point at room temperature and pressure. This was not the case for most reactions performed in this study because water was involved as a product or a reactant. Water was found to condense in the tubes before reaching the syringe. Furthermore, higher hydrocarbons might also have been produced in some experiments, evident from the detection of hydrocarbons heavier than pentane in the gas phase. The low temperature of the dew point of these heavy species would imply that some heavy hydrocarbons would have condensed and existed in the liquid phase. Since the analysis by gas chromatography provided a water-free composition of the gas, the

partial pressures of different species in the gas phase of the reactor were determined by using argon as an internal standard, such that

$$p_i = \frac{x_i}{x_{\mathrm{Ar}}} \times p_{\mathrm{Ar},0} \qquad (1)$$

where p_i is the partial pressure of species *i*, x_i is the mole fraction of species *i* in the syringe, x_{Ar} is the mole fraction of Ar in the syringe and $p_{\mathrm{Ar},0}$ is the partial pressure of argon at the start of the reaction. In most experiments, gas cylinders (of different mixtures of H_2, CO_2 and CO) contained 4% Ar. Hence, $p_{\mathrm{Ar},0}$ could be easily determined by measuring the total pressure of the reactor and multiplying with the known composition of the cylinder. This method of analysis allowed the measurement of the partial pressure of different species in the reactor over time.

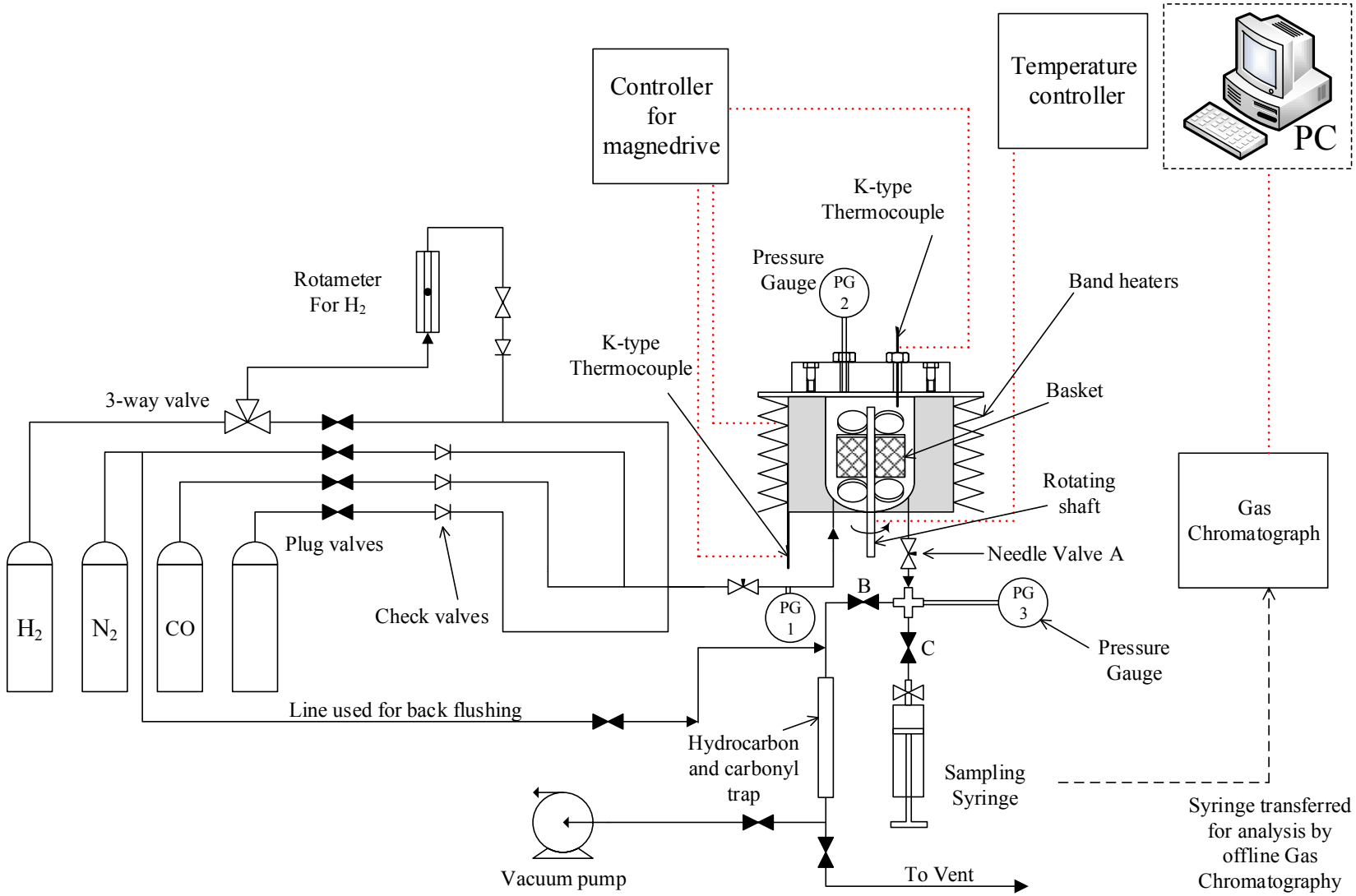

Figure 2. Schematic diagram of the Carberry, spinning-basket reactor. The solid arrows represent the direction of flow of the gases and the red dotted lines represent transmissions of electrical or electronic signals.

3. Results

3.1. Parameters affecting the measurement of kinetics

3.1.1. Control experiment

To determine whether the high-surface area γ-Al_2O_3 (3 mm dia. SA-62125 alumina spheres, Saint-Gobain), used as the support material, was active in the methanation of CO_2, the basket of the reactor was packed with 5.0 g of the support and 5.0 g of non-porous glass beads. The Carberry reactor was sealed and emptied, as described in Section 2.2, and then the pressure was raised to 10 bar absolute by admitting 7.2 bar of H_2, 2.4 bar CO_2 and 0.4 bar Ar into the evacuated vessel, so that the initial partial pressures were $p_{CO_2,0} = 2.4$ bar and $p_{H_2,0} = 7.2$ bar. Samples from the contents of the reactor were removed periodically using a gas-tight syringe and analysed using offline gas chromatography as described above. At both 293 K and 463 K, no significant decreases in p_{CO_2} and p_{H_2} were observed, indicating that the rate of any reaction was negligible. Therefore, the support material used in the synthesis of the Ni/Al_2O_3 catalyst, the interior surface of the reactor and the nickel oxides present in the catalyst could collectively be taken as inert compared to the reduced nickel catalyst.

3.1.2. Catalyst deactivation

It would be challenging to obtain accurate kinetic measurements if the characteristic time for the rate of deactivation of the catalyst were comparable to the rate of methanation in each experiment. Furthermore, significant deactivation would also mean that each batch of catalyst could only be used once and would have to be replaced for each new experiment by a fresh batch of catalyst, which would have go through the reduction process before experimental measurements could be taken. Figure 3 illustrates the change in the partial pressures of CO_2, CH_4, H_2 and C_2H_6 over time for five consecutive, replicate methanation experiments, where the same batch of catalyst was used for the repeated runs. It is clear that the catalyst does not undergo significant deactivation over the total time of the experiments, with a total time-on-stream of about 4.5×10^4 s. Figure 3 (d) shows a small increase in the amount of C_2H_6 produced as the experiment was repeated. This observation was difficult to explain, but the apparent activation of the catalyst towards the production of C_2H_6 could be a result of small changes to the surface of the catalyst after its initial exposure to H_2 and CO_2. Nevertheless,

the amount of C_2H_6 is very much smaller than that of CH_4, which is the primary product, and no significant influence of this change was observed in the profiles of the reactants.

Thus, the insignificant rate of deactivation and good reproducibility meant that experiments could be performed on the same batch of catalyst. As a precaution, the same batch of catalyst was used for no more than 10 experiments before being replaced by a fresh batch. The final experiment on a batch of catalyst was always performed at the same initial conditions, to provide a standard reference point in this study, *viz.* as shown in Figure 3 with initial partial pressures $p_{CO_2,0} = 2.4$ bar, $p_{H_2,0} = 7.2$ bar, $T = 463$ K and $m_{cat} = 5.0$ g, in order to verify that no deactivation has occurred over the length of the past experiments.

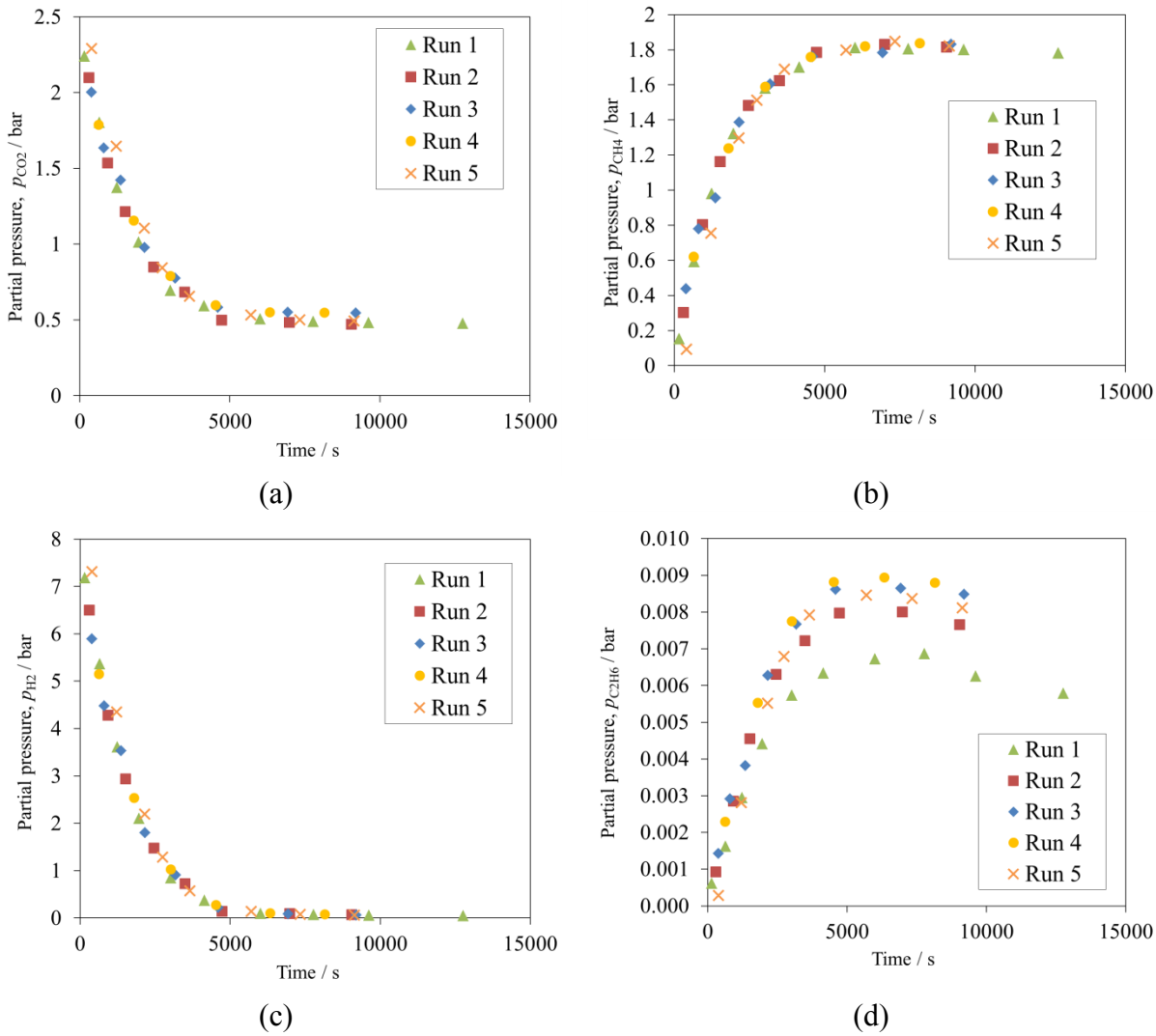

Figure 3. The partial pressure of (a) CO_2, (b) CH_4, (c) H_2 and (d) C_2H_6 as a function of time for five consecutive, replicate batch experiments using the same catalyst. In all experiments, the initial partial pressures of CO_2 and H_2 were $p_{CO_2,0} = 2.4$ bar, $p_{H_2,0} = 7.2$ bar, with $T = 463$ K and $m_{cat} = 5.0$ g.

3.1.3. Heat and mass transfer considerations

Figure 4 shows the experimental results when methanation of CO_2 was undertaken in the batch reactor at different impeller speeds. This was to investigate if there existed significant external gradients of concentration and, or, temperatures between the bulk gaseous phase of the reactor and the external surface of the catalyst pellets. At the extremes, the initial rate of production of methane when the impeller was stationary was about 20% faster than at 9.2 Hz, the maximum speed used in the experiments. Each experiment was repeated twice for each impeller speed. The rate of reaction decreased asymptotically as the impeller speed was increased. At spinning speeds higher than 4.9 Hz, very little difference could be observed between the initial rates. This reduction in rate with increase of stirrer speed was attributed to heat transfer effects, and separate calculations suggested that the small decrease in rate with increase in stirrer speed was due to the enhanced dissipation of the exothermic heat of reaction at higher speeds, and hence a slower rate of reaction. All measurements of kinetics in this study were obtained with a stirrer speed of 9.2 Hz and the results shown in Figure 4 consequently suggest that negligible heat and mass transfer effects were present with the experimental conditions employed.

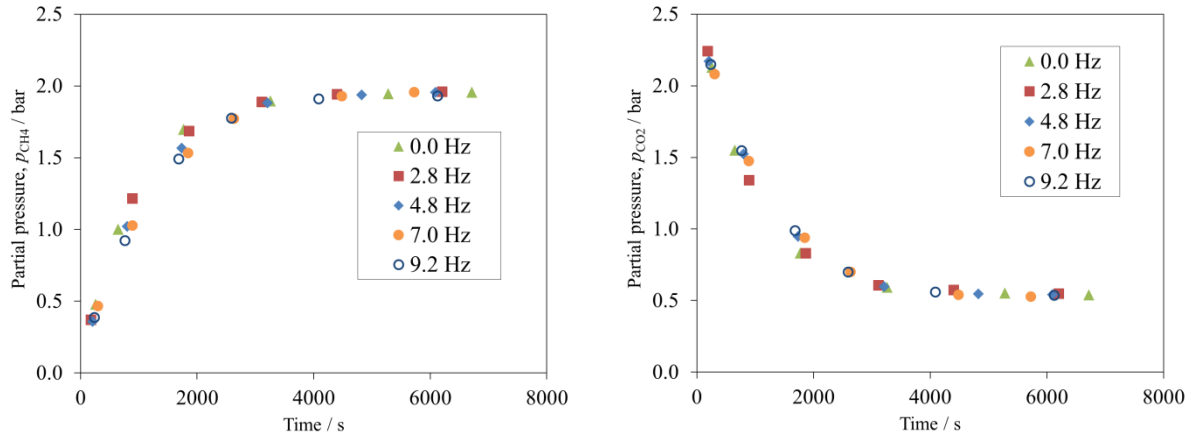

(a) (b)

Figure 4. The change in the partial pressure of (a) CH_4 and (b) CO_2 over time for different stirrer speeds. In all experiments $p_{CO_2,0} = 2.4$ bar, $p_{H_2,0} = 7.2$ bar, $T = 463$ K and $m_{cat} = 5.0$ g.

The Weisz-Prater number, N_{WP}, was used to estimate any potential influence of diffusion within the pores of the catalyst pellet (Weisz and Prater, 1954). The Weisz-Prater criterion states that the value of $N_{WP} < 0.3$ if internal mass transfer limitations are negligible where

$$N_{WP} = \frac{r' \rho_{cat} R_P^2}{C_s D_{eff}}, \qquad (2)$$

C_s being the concentration of CO_2 in mol m^{-3} and D_{eff} the effective diffusivity. N_{WP} was evaluated for CO_2 methanation at 463 K based on the reference conditions of Section 3.1.2. The average pore diameter, d_{pore}, was taken to be 8.9 nm, as determined by BJH analysis and calculated using

$$d_{pore} = \frac{4V_{pore,total}}{A_{pore,total}} \tag{3}$$

where $V_{pore,total}$ is the total pore volume obtained and $A_{pore,total}$ is the corresponding surface area of the pores, assuming that they are cylindrical. Given the small pore diameter, the effective diffusivity, D_{eff}, was taken to be the product of the Knudsen diffusivity of CO_2 and (ε/τ^2), with $\varepsilon = 0.60$ and τ^2 assumed to be 3. Here, ε was determined from the cumulative pore volume of the Al_2O_3 support, accounting for pores ranging from 17 to 300 nm in diameter, of 0.55 cm^3 g^{-1}. The group (ε/τ^2) is appropriate for use with the model of Young and Todd (2005) to model diffusion within the particle of catalyst. N_{WP} was thus 0.09, much smaller than the value at which intra-particle mass transfer is important. Furthermore, the apparent activation energy, as discussed later, was 95 ± 10 kJ mol^{-1}, which is in agreement with previous investigations of CO_2 methanation (Weatherbee and Bartholomew, 1982; van Herwijnen *et al.*, 1973). If significant intraparticle mass transfer had been present, the apparent activation energy would have been significantly smaller. (Levenspiel, 1972).

3.1.4. Effect of total pressure

The stoichiometry of Reaction (1) is such that in a batch reaction the total pressure in the vessel will decrease with progress of reaction. In order to examine the effects of total pressure on the rate of reaction, the reaction was performed for different initial partial pressures of N_2 at $T = 463$ K, $p_{CO_2,0} = 2.4$ bar , $p_{H_2,0} = 7.2$ bar for 5.0 g of catalyst. Figure 5 (a) shows that the total pressure of the system does not affect the rate because the profiles of H_2 with time essentially overlap for different initial partial pressures of N_2. Figure 5 (b) illustrates how S_{CH_4}, the selectivity for CH_4, varies with X_{CO_2}, the conversion of CO_2 at a given time. Here, X_{CO_2} is defined as

$$X_{CO_2} = 1 - \frac{p_{CO_2}}{p_{CO_2,0}} \tag{4}$$

and

$$S_{CH_4} = \frac{p_{CH_4}}{\sum_{i=1}^{5} p_{i,HC}}, \quad (5)$$

where $p_{i,HC}$ is the partial pressure of hydrocarbons with carbon number *i*. The sum of the partial pressures of paraffins from carbon number 1 to 5 was evaluated in the denominator of Eq. (5). In all experiments, S_{CH_4} did not vary with X_{CO_2} and was found to be 0.995 at all conversions. Figure 5 (b) also shows that total pressure did not affect the selectivity of the reaction. The values of S_{CH_4} at $X_{CO_2} = 0$ were found to be slightly lower because p_{CH_4} was small at the start of the reaction and the error incurred by trace hydrocarbons being in the lines of the sampling port or the syringe was relatively large.

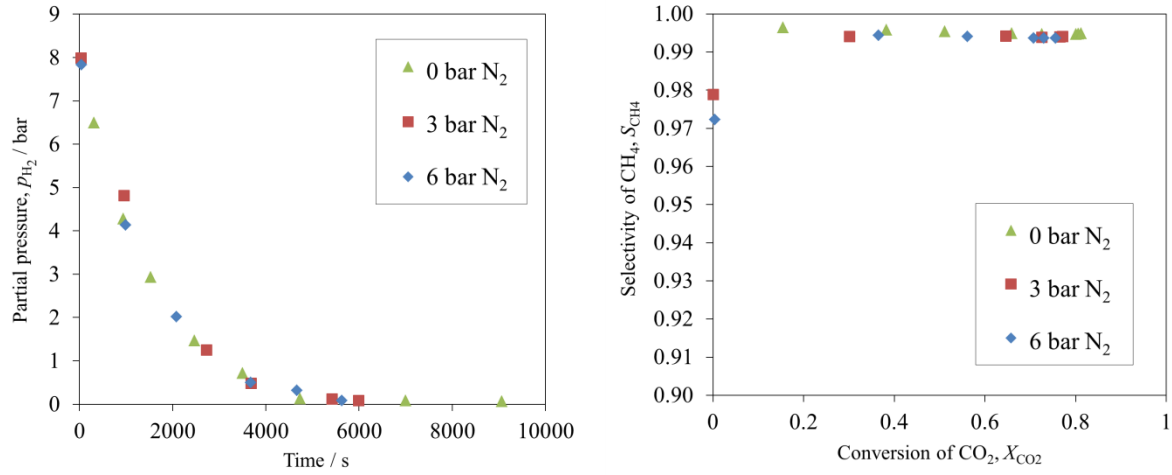

Figure 5. (a) Partial pressure of H_2 over time and (b) the selectivity of CH_4 as a function of the conversion of CO_2 for different initial partial pressures of N_2. In all experiments, $p_{CO_2,0} = 2.4$ bar, $p_{H_2,0} = 7.2$ bar, $T = 463$ K and $m_{cat} = 5.0$ g.

3.2. Measurements of kinetics

The following Sections describe the kinetic measurements performed to elucidate the effects of H_2, CO_2, CH_4 and H_2O on the rate and selectivity of the reaction for the temperature range 443 – 483 K. These experiments were performed by changing the initial partial pressures from the reference initial composition, *i.e.* $p_{CO_2,0} = 2.4$ bar and $p_{H_2,0} = 7.2$ bar, total pressure 10 bar (balance being Ar) and reference temperature, 463 K. The changes in the rate and selectivity were compared by observing the changes in the partial pressures of the reactants and the products. A molar ratio of H_2 to CO_2 of 3:1 was used in the

feed, instead of the stoichiometric ratio 4:1, because it provided a convenient comparison with CO methanation, which has a stoichiometric ratio of 3:1, and is the subject of a later paper.

The experimental results for the reference condition have already been illustrated in Figure 3 for five consecutive, replicated experiments. In Figure 3, CO_2 is in excess, evident from the remaining 0.5 bar of p_{CO_2} after p_{H_2} was depleted. The total amount of p_{CH_4} formed was 1.8 bar. It has already been established that for these conditions, the methane selectivity was very close to unity. Hence, the carbon balance for the experiments could be estimated from the sum of p_{CH_4} and p_{CO_2} at each measurement. This is shown in Figure 6, in which there is seen to be an overall decrease of about 0.1 bar over the length of the experiment, indicating that the maximum error from the removal of the contents of the reactor from sampling was approximately ± 0.1 bar, corresponding to a relative error of 4%.

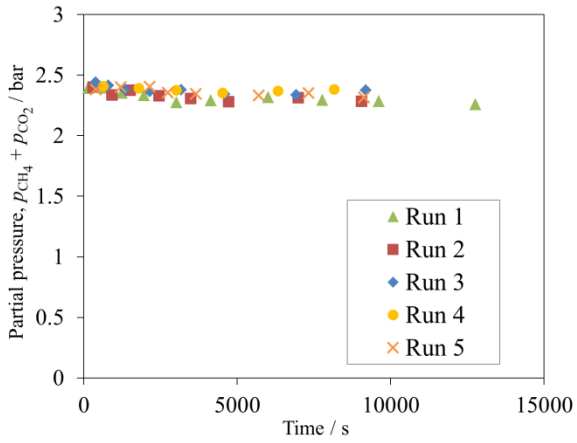

Figure 6. Sum of p_{CH_4} and p_{CO_2} over time for five consecutive, replicated batch experiments using the same catalyst. In all experiments, $p_{CO_2,0} = 2.4$ bar, $p_{H_2,0} = 7.2$ bar, $T = 463$ K and $m_{cat} = 5.0$ g.

3.2.1. Effect of p_{H_2}

The effect of p_{H_2} was investigated by performing CO_2 methanation with different initial partial pressures of H_2, $p_{H_2,0}$, at temperatures 453, 463 and 473 K. To compare the measurements with the reference initial condition of $p_{CO_2,0} = 2.4$ bar and $p_{H_2,0} = 7.2$ bar, the reactor was first filled with an additional quantity of H_2, typically 4 bar H_2, before a mixture of 2.4 bar CO_2 and 7.2 bar H_2 was introduced. This minimised the zero error on the time axis caused by initiating the reaction if the additional H_2 were introduced after the mixture of CO_2 and H_2 had already been admitted to the reactor. Figure 7 illustrates the profiles of CO_2 and CH_4 over time for different initial partial pressures of H_2. Figure 7 (a) shows that the addition

of H_2, while keeping $p_{CO_2,0}$ constant at 2.4 bar, meant that H_2 was in stoichiometric excess compared to CO_2 for experiments with $p_{H_2,0}$ = 11.2 and 15.2 bar. Hence, for these initial conditions, p_{CO_2} eventually dropped to zero. Figure 7 (a) shows that the final amount of p_{CH_4} increased to approximately 2.4 bar, consistent with the total loss of p_{CO_2}. The carbon balance, as determined by the sum of p_{CO_2} and p_{CH_4} and illustrated in Figure 8 (a), was within 5 % of the original p_{CO_2}, *i.e.* 2.4 bar. Figure 8 (b) shows that the selectivity of methane remained at 0.995 for different $p_{H_2,0}$. The initial rate of methanation, deduced either from the rate of increase of p_{CH_4} or the decrease in p_{CO_2} with time, was found to be unaffected by changes in p_{H_2} for 7.2 bar < $p_{H_2,0}$ < 15.2 bar. This can be seen in Figures 7 (a) and (b) where the profiles of CO_2 and CH_4 at low conversions levels, *i.e.* at the start of the reaction when t < 1800 s, are independent of partial pressure of hydrogen in the range considered. However, the profiles of p_{CO_2} and p_{CH_4} for different $p_{H_2,0}$ begin to deviate during the later stages of the reaction, at 1800 < t < 5000 s, during which period the rate was faster for experiments starting with a higher $p_{H_2,0}$. The deviation in the rate of reaction occurred when p_{H_2} dropped below 6 bar, as observed in Figure 7 (c).

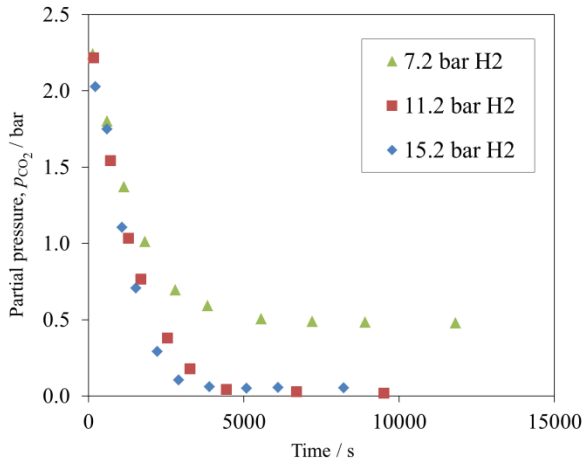

(a)

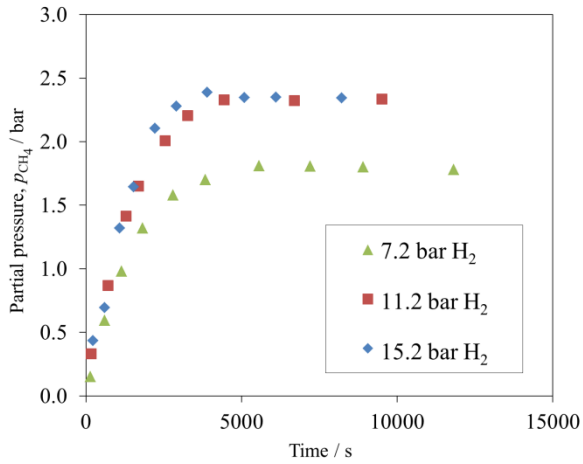

(b)

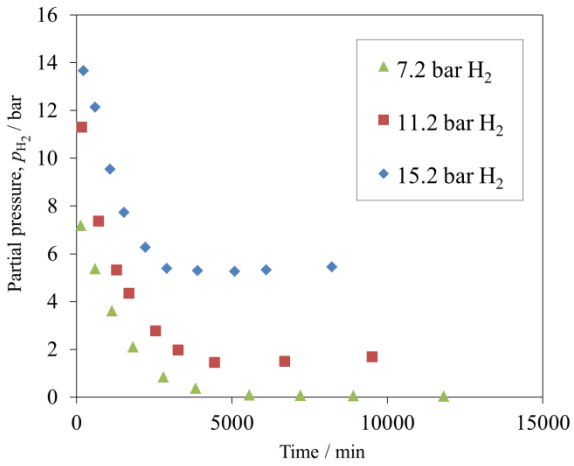

(c)

Figure 7. Partial pressures of (a) CO_2, (b) CH_4 and (c) H_2 with time for different initial partial pressures of H_2, *i.e* $p_{H_2,0}$ = 7.2, 11.2 and 15.2 bar. In all experiments, $p_{CO_2,0}$ = 2.4 bar, T = 463 K and m_{cat} = 5 g.

These observations suggest that at high partial pressures of H_2, the rate of reaction was not affected by changes in p_{H_2}. Increases in the rate with increase in p_{H_2} only appeared at values of p_{H_2} < 6 bar. If the rate of reaction was invariant in p_{H_2} for all values of p_{H_2}, the profiles of p_{CO_2} and p_{CH_4} would overlap for $p_{H_2,0}$ = 11.2 and 15.2 bar, which would be in conflict with the experimental observations here.

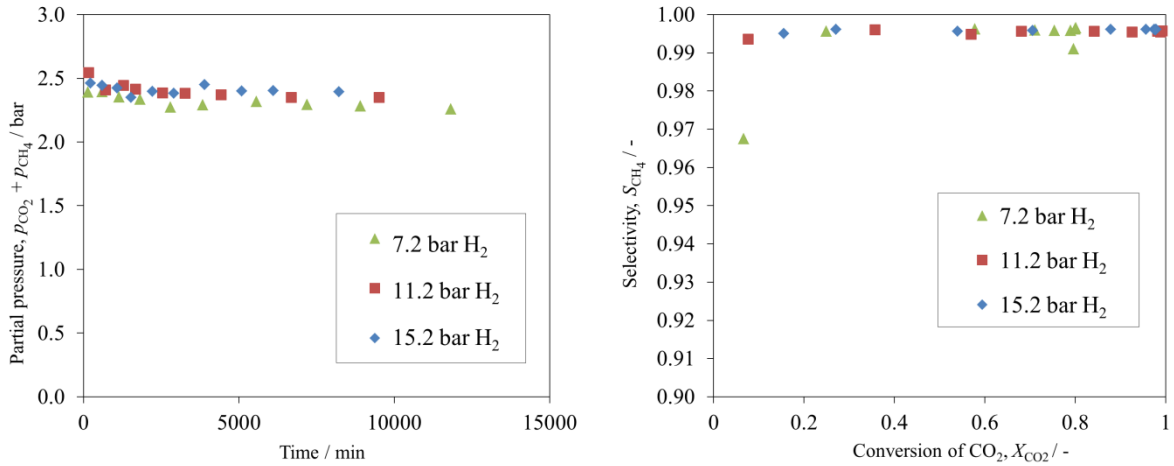

(a) (b)

Figure 8. (a) The sum of p_{CH_4} and p_{CO_2} over time and (d) selectivity of CH_4 as a function of X_{CO_2} for different initial partial pressures of H_2, *i.e* $p_{H_2,0}$ = 7.2, 11.2 and 15.2 bar. In all experiments, $p_{CO_2,0}$ = 2.4 bar, T = 463 K and m_{cat} = 5 g.

3.2.2. Effect of p_{CO_2}

The effect of p_{CO_2} was studied using the same method as outlined in Section 3.2.1, *i.e.* by first introducing additional CO_2 before the introduction of the mixture of CO_2 and H_2. The value of $p_{H_2,0}$ was maintained at 15.2 bar and values of $p_{CO_2,0}$ of 2.4, 2.9 and 3.4 bar were explored at $T = 453 - 473$ K, with 5.0 g of catalyst. Results are shown in Figure 9. There is good evidence that at high p_{CO_2}, as well as high p_{H_2}, the rate is insensitive to changes in p_{CO_2}. This is illustrated in the profiles of H_2, CH_4 and CO_2 in Figure 9 when $t < 2400$ s. However, for low partial pressures of CO_2, *i.e.* when $p_{CO_2} <$ ~0.2 bar, the rate was greater for higher partial pressures of CO_2. In these experiments, S_{CH_4} at complete conversion, *i.e.* $X_{CO_2} = 1$, only decreased from 0.996 for $p_{CO_2,0} = 2.4$ bar to 0.994 for $p_{CO_2,0} = 3.4$ bar. A slight overestimation in the measurement of p_{CO_2} was observed at $t = 0$ s for $p_{CO_2,0} = 2.4$ and 2.9 bar. This error occurred because CO_2 was introduced first into the reactor, filling all the available evacuated space including the sampling lines. Because sampling lines were located a distance away from the impeller, when the reaction was initiated by adding H_2 and further CO_2 and the impeller being turned on, the volume of the sampling line, which had been filled with CO_2, was not mixed well with the bulk phase. The composition of the sample taken at this time did not therefore reflect the true composition of the bulk phase because the sample would have had a higher composition of CO_2. The sampling lines were purged three times before the actual sample was taken but the effect of the dead volume in the sampling lines was not completely eliminated. No such problems were observed for subsequent measurements at later times.

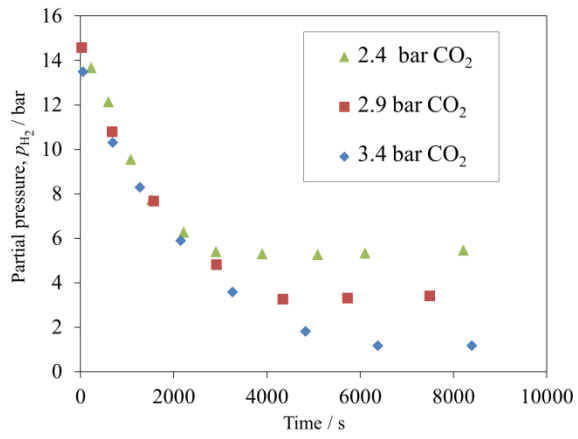

(a)

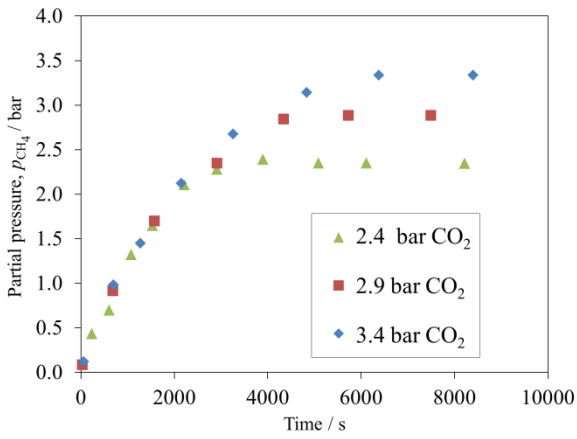

(b)

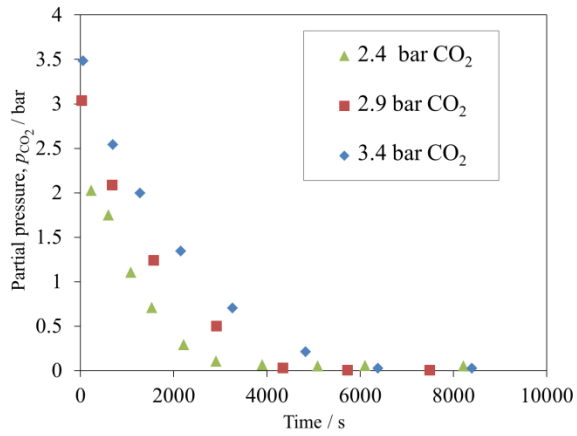

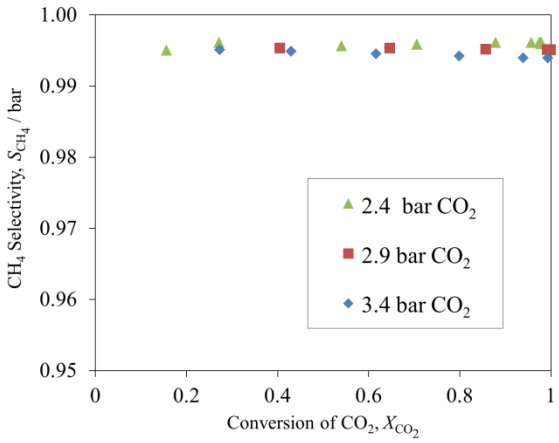

(c)

Figure 9. The partial pressure of (a) H_2, (b) CH_4 and (c) CO_2 versus time for different initial partial pressures of CO_2. (d) The selectivity of CH_4 as a function of the conversion of CO_2. Here, $p_{H_2,0}$ = 15.2 bar, T = 463 K and m_{cat} = 5.0 g.

3.2.3. Effect of p_{CH_4}

Running the reaction in batch means that the products accumulate in the reactor. Hence, it is important to determine whether the main products, *i.e.* CH_4 and H_2O, have any effect on the rate and selectivity of the reaction. As before, it is easiest to elucidate the effect of CH_4 by performing batch reactions with various initial partial pressures of CH_4. The observations are illustrated in Figure 10, where CH_4 is shown to have no effect on the rate of reaction. For the purpose of comparison of measurements from different experiments, the profile of the net change in the partial pressure of CH_4, Δp_{CH_4}, defined as the difference between the measured p_{CH4} at a given time t and that at t = 0, is plotted in Figure 10 (b). Furthermore, no change in selectivity was observed when additional CH_4 was introduced and it is clear that CH_4 simply acts as a spectator molecule in the bulk phase.

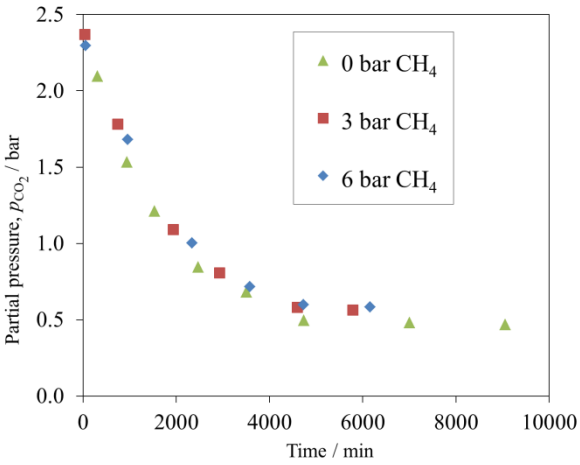

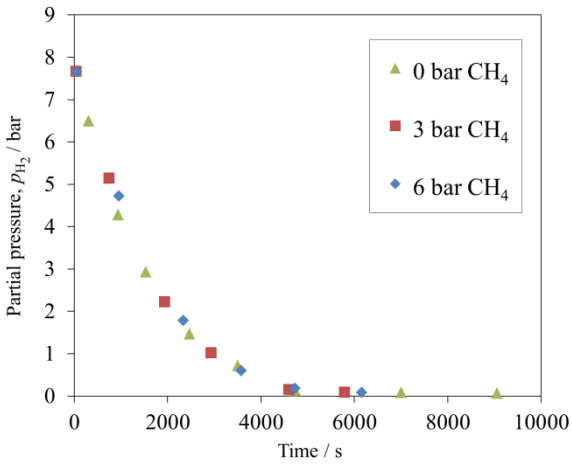

(a) (b)

Figure 10. The partial pressure of (a) CO_2 and (b) H_2 over time for different initial partial pressures of CH_4. In all experiments, $p_{CO_2,0}$ = 2.4 bar, $p_{H_2,0}$ = 7.2 bar, T = 463 K and m_{cat} = 5.0 g.

3.2.4. Effect of p_{H_2O}

Varying the amounts of H_2O present before the start of the CO_2 methanation reaction is difficult experimentally. The introduction of liquid H_2O *via* one of the inlet ports was found to be challenging because the H_2O would vaporise immediately on contact with the hot walls of the reactor and heated lines. The high expansion ratio of H_2O, where 1 ml of H_2O could lead to about 7.2 bar at 473 K if fully vaporised in the reactor, meant that such a procedure was not only operationally dangerous but also it was difficult to obtain a desired partial pressure of H_2O, p_{H_2O}.

It has already been established that the CO_2 methanation reaction over the 12 wt% Ni/γ-Al_2O_3 has a high selectivity for CH_4. This means that performing a batch reaction to completion with a stoichiometric ratio of H_2 to CO of 4:1 would yield a reactor containing mainly CH_4 and H_2O. Since CH_4 was had no effect on the rate and selectivity of the reaction, if additional CO_2 and H_2 were introduced into the reactor, the subsequent measurements would account for the effect of H_2O on the reaction. In this study, 1 bar of CO_2 was added to 4 bar of H_2 in order to obtain a nominal $p_{H_2O,0}$, the initial partial pressure of H_2O, of 2 bar. A $p_{H_2O,0}$ of 4 bar was obtained with 2 bar CO_2 and 4 bar H_2. The reaction was deemed complete when no further drop in the total pressure was observed on the pressure gauge. This was also verified by checking that negligible amounts of H_2 and CO_2 were present in the gas chromatogram in a separate experiment with the same initial partial pressures of CO_2 and H_2. In order to decrease the errors introduced from sampling, for the experimental results presented here, no samples were taken from the reactor before additional CO_2 and H_2 were introduced.

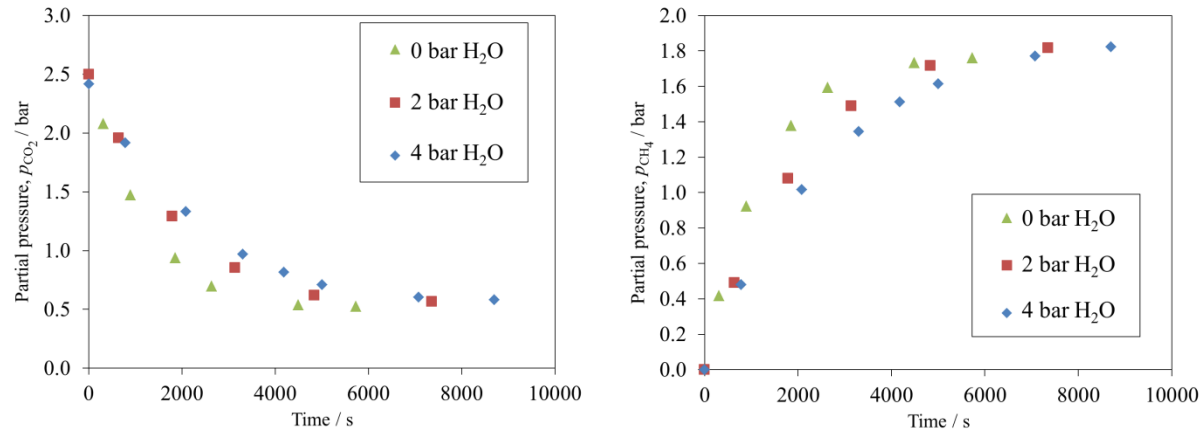

(a) (b)

Figure 11. Partial pressure of (a) CO_2 and (b) CH_4 *versus* time for different initial partial pressures of H_2O. In all experiments, $p_{CO_2,0}$ = 2.4 bar, $p_{H_2,0}$ = 7.2 bar, T = 463 K and m_{cat} = 5.0 g.

In this way, it was found that H_2O inhibited the rate of methanation of CO_2 significantly. This is illustrated in the profiles of CO_2 and CH_4 in Figures 11 (a) and (b). Figure 12 shows no observable change in CH_4 selectivity as partial pressures of H_2O are increased. Unlike the effect of CO_2 and H_2, the effect of H_2O on the rate of reaction could be seen from the beginning of the reaction. The initial rate of production of CH_4 decreased from 2.0×10^{-6} mol_{CH_4} s^{-1} g^{-1} when $p_{H_2O,0}$ = 0 to 1.4×10^{-6} mol_{CH_4} s^{-1} g^{-1} with $p_{H_2O,0}$ = 2 bar, a decrease of 30 %. However, the rate only fell to 1.0×10^{-6} mol_{CH4} s^{-1} g^{-1}, a further decrease of only 20% when $p_{H_2O,0}$ = 4 bar, suggesting that the rate is less sensitive to the presence of water at higher p_{H_2O}. It is evident that the gradual decrease in the rate of CO_2 methanation, as observed in a batch reactor, is not only because of the decreasing partial pressures of the reactants but also because of the increase in p_{H_2O}. Since even small levels of H_2O were found to inhibit the rate of reaction, it is important that this effect is accounted for when interpreting the measurements at higher conversions in the batch reactor.

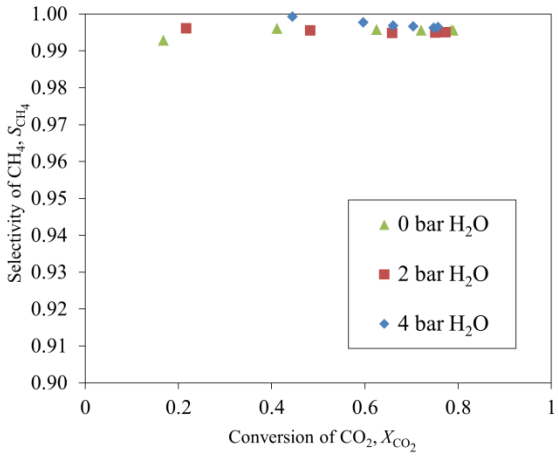

Figure 12. The selectivity CH_4 as a function of the conversion of CO_2 for different initial partial pressures of H_2O. In all experiments, $p_{CO_2,0}$ = 2.4 bar, $p_{H_2,0}$ = 7.2 bar, T = 463 K and m_{cat} = 5.0 g.

3.2.5. Effect of temperature

Figure 13 shows the variation of CO_2, H_2 and CH_4 over time for $p_{CO_2,0}$ = 2.4 bar, $p_{H_2,0}$ = 7.2 bar at different reaction temperatures, *i.e.* from 443 – 483 K. Figure 14 (a) shows a small change in selectivity of CH_4 over the temperature range , increasing from 0.990 at 443 K to about 0.997 at 483 K, at X_{CO_2} = 0.8. However, the effect of this increase in the selectivity of CH_4 with temperature on the overall consumption ratio of H_2 to CO_2 is negligible. This is evident from Figure 13 (a), where the excess p_{CO_2} remained at ~0.5 bar, at all temperatures, after p_{H_2} was depleted. The sum of p_{CO_2} and p_{CH_4} accounted for the majority of the carbon balance at all temperatures explored, as shown in Figure 14 (b). The sum of p_{CO_2} and p_{CH_4} generally increased with temperature because of the slight shift in CH_4 selectivity at higher temperatures. Nevertheless, even at the lowest temperature of 443 K, the sum of p_{CO_2} and p_{CH_4} still accounted for 92% of the initial p_{CO_2} .

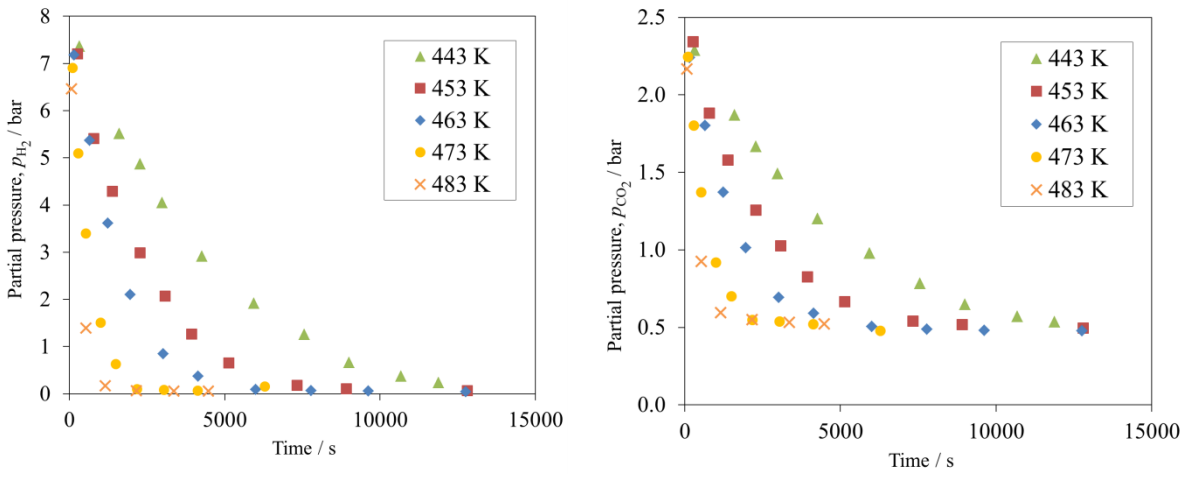

(a) (b)

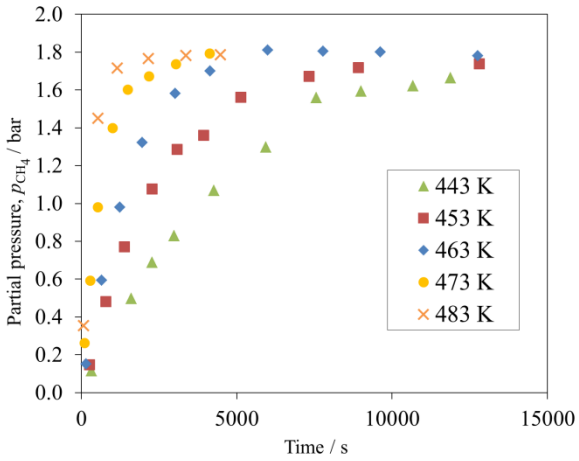

(c)

Figure 13. Partial pressure of (a) H_2, (b) CO_2 and (c) CH_4 *versus* time at different reaction temperatures. In all experiments, $p_{CO_2,0}$ = 2.4 bar, $p_{H_2,0}$ = 7.2 bar and m_{cat} = 5.0 g.

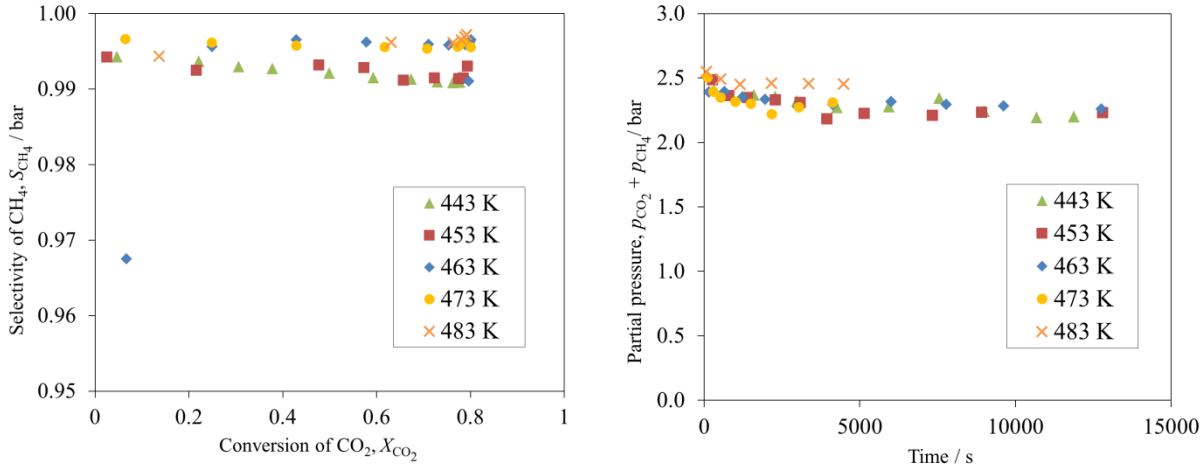

(a) (b)

Figure 14. (a) Selectivity of CH_4 as a function of the conversion of CO_2 and (b) the sum of p_{CH_4} and p_{CO_2} for different temperatures. In all experiments, $p_{CO_2,0}$ = 2.4 bar, $p_{H_2,0}$ = 7.2 bar and m_{cat} = 5.0 g.

3.3. Temperature-programmed studies

Following the batch reactions in the Carberry reactor, the spent sample of catalyst was removed and stored in a capped glass jar. Temperature programmed desorption (TPD) was performed on the stored catalyst in the CATLAB apparatus, where 40 ml/min (measured at room temperature and pressure) of He was passed through 50 mg of the spent catalyst in a cylindrical tubular reactor. The sample was held at 120°C for 1 hour under He before the temperature was increased at a ramp rate of 10°C/min. Figure 15 shows the evolution of H_2O, CO_2 and CH_4 in the off-gas, measured by a mass spectrometer, as a function of temperature. The calibration of the signals of the mass spectrometer was challenging because the absolute values of the signals are dependent on parameters other than the quantity of material, *e.g.* the total pressure within the spectrometer. As such there was a day-to-day variation in the signal intensity. The interpretation of the results from CATLAB was therefore performed by comparing the rate of change of the signals. There appeared to be three main regions for the evolution of CO_2: a shoulder at 200°C, a main peak at 300°C and a smaller peak at 350°C. The profile of water is extremely broad, as seen. The rate of evolution of methane was rather similar to that of water but its measurement was unlikely to have been accurate since the atomic mass of methane is identical to that of an oxygen fragment. No significant evolution of H_2 was observed between 100 and 700°C. The import of these observations is discussed in Section 5, below, after the modelling has been introduced and discussed.

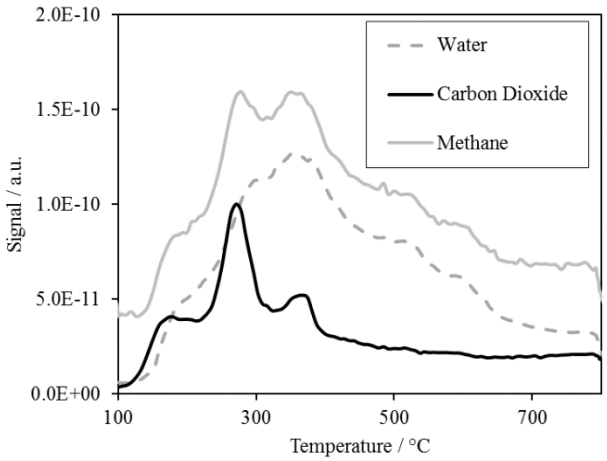

Figure 15. The profiles of H_2O, CO_2 and CH_4 *versus* temperature in a temperature-programmed desorption of the spent 12 wt% Ni/γ-Al_2O_3 after CO_2 methanation reaction in the batch reactor. Following a drying period at 120°C, the temperature was increased at a rate of 10°C/min under a flow of 40 ml/min (measured at room temperature and pressure) He.

3.4. DRIFTS measurements

Here, 50 mg of fresh, passivated 12 wt% Ni/γ-Al_2O_3 catalyst was packed as a differential bed and reduced at 450°C for 2 hours under 100 ml/min (at room temperature and pressure) of H_2. Following the reduction, a mixture containing 0.24 bar CO_2, 0.72 bar H_2 and 0.04 bar Ar was passed across the differential bed at a flow rate of 100 ml/min (at room temperature and 1 bar total pressure). Figure 16 illustrates the main features of the IR spectrum obtained at 463 K at steady-state under reaction conditions. The identification of the species was based on Fujita *et al.* (1993), who studied supported Ni on alumina using DRIFTS. The absorbance bands at 2050, 1920 and 1840 cm^{-1} were attributed to straight and bridged carbonyl groups on the surface of the catalyst. The presence of formates was also detected, reflected in the large peaks at 1620, 1590, 1390, 1350, 1330 and 2890 cm^{-1}. Following the reaction at 463 K under CO_2 and H_2, the inlet flow was changed to 100 ml/min (at room temperature and pressure) of H_2 and spectra of the surface of the catalyst were obtained periodically. The carbonyl peaks at 2050, 1920 and 1840 cm^{-1} decreased in magnitude very quickly and disappeared after approximately 5 mins. However, the formate groups persisted even after 40 minutes under a flow of H_2, indicating that they were bound more strongly to the surface of the catalyst than the carbonyl groups and were less reactive than the carbonyl species with H_2.

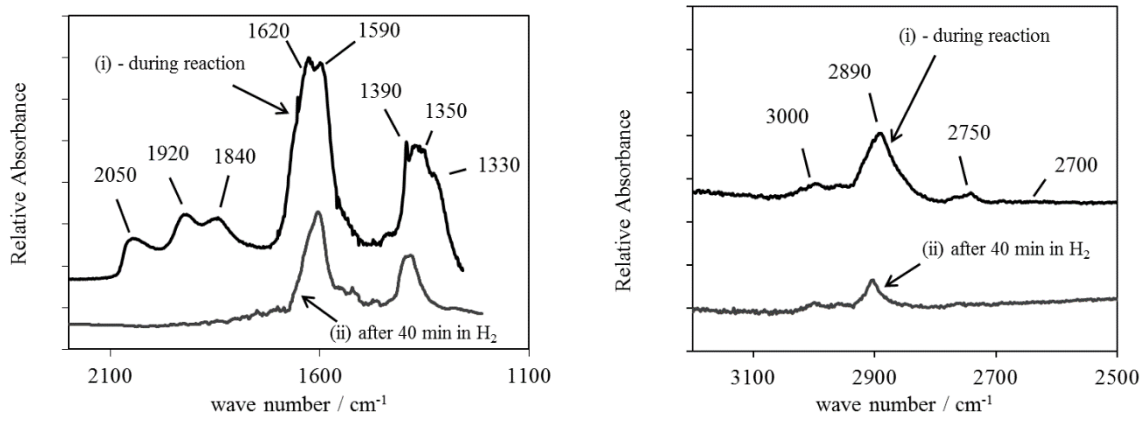

Figure 16. Infrared spectra of the adsorbed species in the range from (a) 1100 – 2200 cm^{-1} and (b) 2500 – 3300 cm^{-1} formed on reduced 12 wt% Ni/Al_2O_3 in flow of 100 ml/min (at room temperature and pressure) of 0.24 bar CO_2, 0.72 bar H_2 and 0.04 bar Ar at 463 K. The spectrum of the catalyst under He was used as the background.

4. Modelling

4.1.1. Reactor model

Reaction (1) has been established as the main reaction in CO_2 methanation over the temperature range 443 – 493 K. Negligible levels of CO were detected in the bulk phase and the reaction was found to be at least 99.0% selective for methane. Therefore, it is reasonable to develop the model of the reactor based on the stoichiometry of the single Reaction (1). It has already been established in the above that there were no significant intra-particle or extra-particle gradients in concentration and temperature in the catalyst pellets. Hence, the transient changes of p_{CO_2}, p_{H_2}, p_{CH_4} and p_{H_2O} in the Carberry spinning-basket reactor could be modelled as a set of four ordinary differential equations:

$$\frac{dp_{CO_2}}{dt} = -\frac{m_{cat}RT}{V_{reactor}\times 10^5} r' \tag{6}$$

$$\frac{dp_{H_2}}{dt} = -\frac{4m_{cat}RT}{V_{reactor}\times 10^5} r' \tag{7}$$

$$\frac{dp_{CH_4}}{dt} = \frac{m_{cat}RT}{V_{reactor}\times 10^5} r' \tag{8}$$

$$\frac{dp_{H_2O}}{dt} = \frac{2m_{cat}RT}{V_{reactor}\times 10^5} r' \tag{9}$$

where p_{CO_2}, p_{H_2}, p_{CH_4} and p_{H_2O} are the partial pressures of CO_2, H_2, CH_4 and H_2O respectively in bar, r' is the rate of Reaction (1) in mol s^{-1} g_{cat}^{-1}, t is time in seconds, m_{cat} is the mass of the catalyst in the reactor in grams and $V_{reactor}$ is the volume of the reactor in m^3. The initial conditions for the experiments were

$$\text{for } t = 0, \qquad p_i = p_{i.0}\,. \tag{10}$$

where p_i is the partial pressure of component i in bar and p_{i0} is the initial partial pressure of species i. Given a rate expression for r', which could be a function of p_{CO_2}, p_{H_2}, p_{CH_4} and p_{H_2O} at a given temperature, Equations (6) to (10) were solved using the MATLAB solver ode45 to give the variation of the partial pressure of CO_2, H_2, CH_4 and H_2O over time for comparison with the experimental results.

4.1.2. Kinetic modelling

This Section investigates the validity of different rate expressions for CO_2 methanation using kinetic models based on a Langmuir-Hinshelwood approach. The active sites for the reaction were assumed to be identical and their distribution uniform throughout the catalyst. It was assumed that CO_2 methanation occurred *via* the dissociative adsorption of CO_2 (Weatherbee and Bartholomew, 1982). The sequence of elementary steps is outlined in Reactions (2) to (8):

$$H_{2(g)} + 2\theta \underset{k_{-1}}{\overset{k_1}{\rightleftharpoons}} \tag{R2}$$

$$CO_{2(g)} + 2\theta \underset{k_{-2}}{\overset{k_2}{\rightleftharpoons}} \theta_O \tag{R3}$$

$$\theta_{CO} \underset{k_{-3}}{\overset{k_3}{\rightleftharpoons}} (g) + \theta \tag{R4}$$

$$\theta_{CO} + \theta \xrightarrow{k_4} \theta_C + \theta_O \tag{R5}$$

$$\theta_O + \theta_H \underset{k_{-5}}{\overset{k_5}{\rightleftharpoons}} \theta \tag{R6}$$

$$\theta_{OH} + \theta_H \xrightarrow{k_6} \theta_{H_2O} + \theta \tag{R7}$$

$$\theta_{H_2O} \underset{k_{-7}}{\overset{k_7}{\rightleftharpoons}} (g) + \theta \tag{R8}$$

where k_i and k_{-i} are the forward and reverse rate of reaction for the specified elementary step and θ_i presented adsorbed species i on an active site θ. Further steps include hydrogenation

of the θ_{CO} and the subsequent desorption of θ_{CH_4} to form CH_4 following from Reaction (5). Thus:

$$\theta_C + \theta_H \rightleftharpoons \theta_{CH} + \theta$$

$$\theta_{CH} + \theta_H \rightleftharpoons \theta_{CH_2} + \theta$$

$$\theta_{CH_2} + \theta_H \rightleftharpoons \theta_{CH_3} + \theta$$

$$\theta_{CH_3} + \theta_H \rightleftharpoons \theta_{CH_4} + \theta$$

$$\theta_{CH_4} \rightleftharpoons CH_{4(g)} + \theta .$$

A number of different rate expressions were derived from this sequence of elementary steps, depending on assumptions about the rate-limiting step and the most abundant species on the surface of the catalyst. Table 1 gives four examples of rate expressions derived based on different rate-limiting steps and the most abundant surface species. It should be noted that some of the kinetic parameters in Eqs. (11)-(14) are a composite of a number of rate and equilibrium constants, produced during the derivations. It is beyond the scope of this study to determine the values of all of the individual constants and the investigation is limited to the evaluation of the four main kinetic parameters *a*, *b*, *c* and *d*. Three other rate expressions for CO_2 methanation, proposed by other investigators, are given in Table 2. The derivations of Eqs. (11) and (12) were largely based on the study by Weatherbee and Bartholomew (1982). However, in this study, H_2O was included as a dominant surface species in order to account for its inhibition on the rate of reaction, as observed in the experiments.

4.1.3. Model discrimination

Of course, not all the rate expressions in Tables 1 and 2 agree with the experimental results obtained in the present research. Equations (13) and (14) predict a finite rate when respectively either p_{CO_2} or p_{H_2} is zero. This is in conflict with the experimental evidence here. Figure 7 clearly illustrates that there was no further decrease in p_{CO_2} when H_2 was depleted and, similarly, Figure 9 shows no decrease in p_{H_2} when CO_2 was depleted. The same argument applies to Eq. (16).

The power law expression proposed by Chiang and Hopper (1983), Eq. (15), predicts that the rate of reaction would continue to increase indefinitely with p_{H_2} and p_{CO_2}. This is

contrary to the experimental results in Sections 3.2.1 and 3.2.2, where the rate of reaction was not affected by p_{H_2} and p_{CO_2} after values of p_{H_2} and p_{CO_2} exceeded certain threshold values. The inhibition of the rate of reaction by steam, evident in Section 3.2.4, was also not accounted for by Eqs. (13) – (17).

Table 1. Rate expressions based on different assumptions of the rate limiting step and the most abundant surface species. p_i is the partial pressure of component i and r_{CH4} is the rate of production of CH_4.

Model	Rate expression	Rate-limiting step	Most abundant surface species	
I	$\frac{a_{\mathrm{I}} p_{\mathrm{CO_2}}{}^{0.5} p_{\mathrm{H_2}}{}^{0.5}}{\left(1+b_{\mathrm{I}}\sqrt{p_{\mathrm{H_2}}}+c_{\mathrm{I}} p_{\mathrm{CO_2}}{}^{0.5} p_{\mathrm{H_2}}{}^{0.5}+d_{\mathrm{I}} p_{\mathrm{H_2O}}\right)^2}$	CO dissociation	H, CO and H_2O	(11)
II	$\frac{a_{\mathrm{II}} p_{\mathrm{CO_2}}{}^{0.5} p_{\mathrm{H_2}}{}^{0.5}}{\left(1+b_{\mathrm{II}}\left(\frac{p_{\mathrm{CO_2}}}{p_{\mathrm{H_2}}}\right)^{0.5}+c_{\mathrm{II}} p_{\mathrm{CO_2}}{}^{0.5} p_{\mathrm{H_2}}{}^{0.5}+d_{\mathrm{II}} p_{\mathrm{H_2O}}\right)^2}$	CO dissociation	CO, O and H_2O	(12)
III	$\frac{a_{\mathrm{III}} p_{\mathrm{H_2}}}{\left(1+b_{\mathrm{III}}\sqrt{p_{\mathrm{CO_2}}}+c_{\mathrm{III}}\sqrt{p_{\mathrm{H_2}}}\right)^2}$	Adsorption of H_2	H, CO and O	(13)
IV	$\frac{a_{\mathrm{VI}} p_{\mathrm{CO_2}}}{\left(1+b_{\mathrm{VI}}\sqrt{p_{\mathrm{CO_2}}}+c_{\mathrm{VI}}\sqrt{p_{\mathrm{H_2}}}\right)^2}$	Adsorption of CO_2	H, CO and O	(14)

Table 2. Some rate expressions proposed by other investigators for CO_2 methanation.

Rate expression	Reference	
$r' = k p_{\mathrm{H_2}}^{0.21} p_{\mathrm{CO_2}}^{0.66}$	Chiang and Hopper (1983)	(15)
$r' = \frac{k p_{\mathrm{CO2}}}{1+K_{\mathrm{CO_2}} p_{\mathrm{CO2}}}$	van Herwijnen *et al.* (1973)	(16)
$r' = \frac{k\sqrt{p_{\mathrm{CO_2}}}\sqrt{p_{\mathrm{H_2}}}}{\left(1+K_1\frac{\sqrt{p_{\mathrm{CO_2}}}}{\sqrt{p_{\mathrm{H_2}}}}+K_2\sqrt{p_{\mathrm{CO_2}}}\sqrt{p_{\mathrm{H_2}}}+K_3 p_{\mathrm{CO}}\right)^2}$	Weatherbee and Bartholomew (1982)	(17)

The two most plausible rate expressions are those of Model I and II, *i.e.* Eqs. (11) and (12). Further comparison of these two models was performed here by substituting the rate expressions into the model of the reactor, given in Section 4.1.1, and comparing the predictions with the experimental measurements at different conditions. To do this, the parameters, a, b, c and d for each model were estimated based on a least-squares

minimisation developed in MATLAB. Thus, the agreement between the model and the experimental results was studied by comparing the solution of the system of ODEs with the temporal variation of the partial pressures of the various species measured in the batch experiments. In the minimisation routine, the difference, $d_i(t)$, between these values were compared for each iteration at time *t* with the experimental measurements for p_{CO_2}, p_{H_2} and p_{CH_4}, such that

$$d_i(t) = p_{i,\text{model}}(t) - p_{i,\text{exp}}(t) \tag{18}$$

where $p_{i,\text{model}}(t)$ is the partial pressure of species *i* determined by the solution of the ODEs and $p_{i,\text{exp}}(t)$ is the partial pressure of species *i* measured experimentally. The sum of all the squares of each component was evaluated at a given time, *t*, such that

$$D = \sum_i \left(d_i(t)\right)^2 . \tag{19}$$

The values of the parameters *a*, *b*, *c* and *d* of Model I and II, were obtained by minimising the value *D* using the MATLAB optimisation routine lsqnonlin.

4.1.4. Model I

The derivation of Model I was based on the assumption that the rate-determining step is the dissociation of the CO and that the most abundant species on the surface of the catalyst are adsorbed H, CO and H_2O. Since, the parameter b_I is, in fact, the adsorption equilibrium constant of hydrogen on the surface of the catalyst, its value was obtained from Sehested *et al.* (2005), who studied the methanation of CO over a $Ni/MgAl_2O_4$ catalyst, thus

$$b_I = 7.7\times10^{-4}\exp\left(\frac{43000}{RT}\right). \tag{20}$$

consistent with partial pressures expressed in bar. Alstrup (1995) and Aparicio (1997) have also reported values of b_I. There is good agreement between the b_I obtained by Alstrup (1995) and Sehested (2005). The values of b_I obtained by Aparicio (1997) were an order of magnitude larger than those given by Eq. (20). However, the values of the heat of adsorption determined by Aparicio (1997) were found by to be in good agreement with Eq. (20) with the pre-exponential factor being responsible for the discrepancy between the reported values of b_I. With the value of b_I predetermined, only three parameters were left to be determined using the optimisation routine. Figure 17 compares the result of the least-squares minimisation

routine for different initial p_{H_2}. It is clear that, because of the high value of b_I, the model predicts an increase in the rate of reaction at low p_{H_2}. The modelling results for $p_{H_2,0} = 7.2$ bar show that the profile of p_{H_2} is approximately linear with time, in stark contrast with the experimental measurements where the rate decreased at higher conversions. Furthermore, the least-squares minimisation routine resulted in negative values of c_I, which have no physical interpretation.

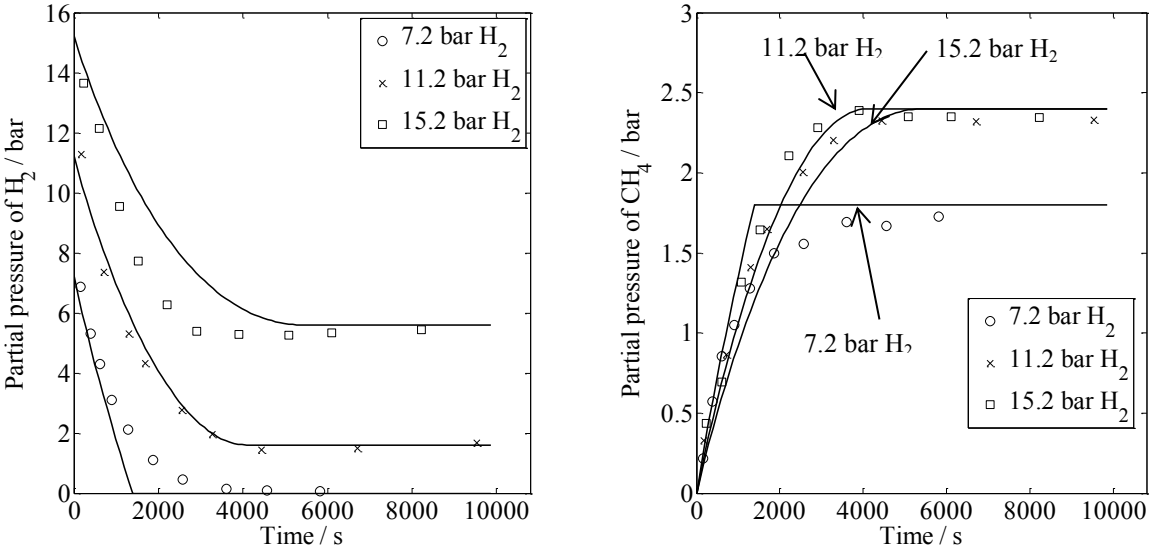

(a) (b)

Figure 17. Comparison between the modelling results (Model I, Eq. (20)) and the experimental results for different initial partial pressure of H_2. (a) shows the partial pressure of H_2 with time and (b) the partial pressure of CH_4 with time. $T = 463$ K, $p_{H_2,0} = 7.2$ bar, $p_{CO_2,0} = 2.4$ bar and $m_{cat} = 5$ g..

To proceed, the pre-exponential value of b_I was allowed to vary in the least-squares minimisation routine. Table 3 gives the results of the optimisation. Figure 18 shows that by relaxing the pre-exponential term of b_I, a much better agreement was obtained with the experimental measurements. The agreement was verified with measurements taken from 443 – 483 K and the values of the kinetic constants are given in Table 3. Assuming that these parameters follow the Arrhenius relationship, the values of activation energy and heat of adsorption were obtained, given in Table 4. While the agreement with the experimental results was good, the pre-exponential factor b_0 was found to be 5×10^{-7} bar$^{-0.5}$, very much smaller than that reported by Sehested *et al.* (2005). It could be argued that the surface of the catalyst in this study is different to that in other investigations, which were mainly studies

where high p_{CO_2} were involved. Alternatively, atomic H might not be one of the most abundant species on the surface of the catalyst under conditions for CO_2 methanation, which would explain the low level of affinity for the surface suggested by the value of b_I determined here.

Table 3. Values of parameters from a fit of Model I to the experimental results.

Temp / K	a_I / mol bar^{-1} s^{-1}	b_I / bar$^{-0.5}$	c_I / bar^{-1}	d_I / bar^{-1}
443	$(2.2 \pm 0.2) \times 10^{-5}$	0.059 ± 0.006	0.101 ± 0.002	0.20 ± 0.01
453	$(3.8 \pm 0.1) \times 10^{-5}$	0.046 ± 0.002	0.091 ± 0.002	0.16 ± 0.01
463	$(6.1 \pm 0.3) \times 10^{-5}$	0.036 ± 0.004	0.082 ± 0.003	0.12 ± 0.03
473	$(9.0 \pm 0.5) \times 10^{-5}$	0.028 ± 0.004	0.074 ± 0.008	0.12 ± 0.02
483	$(2.0 \pm 0.3) \times 10^{-4}$	0.023 ± 0.011	0.067 ± 0.022	0.10 ± 0.01

Table 4. Values of the activation energy, heat of adsorption and the corresponding pre-exponential factors of the parameters for Model I.

a_0	b_0	c_0	d_0
49.4×10^6 mol bar^{-1} s^{-1}	5.0×10^{-7} bar$^{-0.5}$	5.6×10^{-2} bar^{-1}	4.6×10^{-4} bar^{-1}

ΔE_a	ΔH_b	ΔH_c	ΔH_d
92 kJ mol^{-1}	- 43 kJ mol^{-1}	- 1.5 kJ mol^{-1}	- 21.5 kJ mol^{-1}

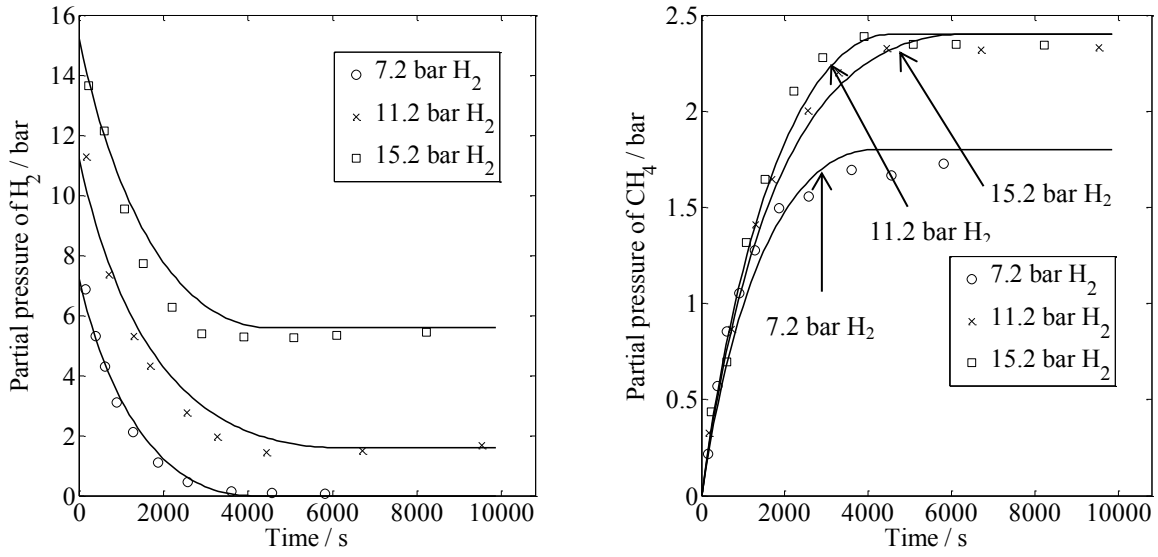

(a) (b)

Figure 18. Comparison of the modelling results (Model I, with pre-exponential for Eq. 920) allowed to vary) and the experimental results for different initial partial pressure of H_2. (a) shows the partial pressure of H_2 with time and (b) the partial pressure of CH_4 with time. $T = 463$ K, $p_{H_2,0} = 7.2$ bar, $p_{CO_2,0} = 2.4$ bar and $m_{cat} = 5$ g. The parameters in the kinetic model are given in Table 4.

4.1.5. Model II

The main difference between Model II and Model I is that Model II, given by Eq. (12), assumes that the most abundant species on the surface of the catalyst are H_2O, O and CO. The rate-limiting step of the reaction remains the dissociation of CO. As noted above, the derivations of these equations were largely based on Weatherbee and Bartholomew's (1982) investigation but were extended in this research to account for the inhibitory effect of H_2O on the rate of reaction. Weatherbee and Bartholomew (1982) obtained values of b_{II} over the range 500 – 600 K, and summarised their findings by

$$b_{II} = 4.27 \times 10^{-7} \exp\left(\frac{46000}{RT}\right). \tag{21}$$

Given that their experiments were performed using a differential reactor, the conversion of CO_2, X_{CO_2}, was low. Hence, it is reasonable to assume that the effect of H_2O in their experiments was negligible because p_{H_2O} could be taken to be small. In the present work, the values of b_{II} at different temperatures were based on the extrapolation of Eq. (21) to temperatures of 443 – 483 K. The other parameters a_{II}, c_{II} and d_{II} were obtained by the least-squares fit algorithm, as described previously. The modelling results showed that c_{II} was largely invariant over the range 443 – 483 K, with an average of 0.16 ± 0.02 bar^{-1}. It should be noted that c_{II} is a composite of a number of kinetic and equilibrium constants: it is interesting that the resulting net "activation energy", although not a true activation energy in the kinetic sense, appeared to be zero. In fact, the values of c_{II} obtained by Weatherbee and Bartholomew (1982) did not show a clear trend with temperature, with a maximum value of 0.143 at 550 K. The values of the various kinetic constants obtained in the present work for Model II are given in Table 5 and the estimated values of activation energies, heats of adsorption and pre-exponential factors in Table 6.

Table 5. Values of parameters from the least-squares fit of Model II to the experimental results.

Temp / K	a_{II} / mol bar^{-1} s^{-1}	b_{II} / -	d_{II} / bar^{-1}
443	$(3.54 \pm 0.07) \times 10^{-5}$	0.039	0.23 ± 0.01
453	$(4.92 \pm 0.05) \times 10^{-5}$	0.051	0.19 ± 0.01
463	$(8.38 \pm 0.08) \times 10^{-5}$	0.066	0.16 ± 0.01
473	$(1.31 \pm 0.07) \times 10^{-4}$	0.085	0.13 ± 0.02
483	$(2.88 \pm 0.08) \times 10^{-4}$	0.110	0.11 ± 0.02

Table 6. Values of the activation energy, heat of adsorption and the corresponding pre-exponential factors for the parameters in Model II.

$a_{II,0}$	$b_{II,0}$	$c_{II,0}$	$d_{II,0}$ bar^{-1}
2.3×10^{6} mol bar^{-1} s^{-1}	4.3×10^{-7}	0.16 bar^{-1}	3.4×10^{-5} bar^{-1}

ΔE_a	ΔH_b	ΔH_c	ΔH_d
95 kJ mol^{-1}	-46 kJ mol^{-1}	-	-32 kJ mol^{-1}

For each set of initial conditions explored, all the experimental and modelling profiles of the three components, *i.e.* CO_2, H_2 and CH_4, were compared. For illustration, Figure 19 shows p_{H_2} and p_{CH_4} as a function of time at $T = 473$ K for different initial partial pressures of H_2 while Figure 20 illustrates p_{CO_2} and p_{CH_4} versus time at $T = 463$ K for different initial partial pressures of H_2O. It is clear that Model II correctly predicts a number of experimental observations. At high p_{CO_2} and p_{H_2}, the rate is largely unaffected by changes in p_{CO_2} and p_{H_2}, which is clearly observed in Figure 19 (a) and (b) at $t < 1000$ s. Furthermore, the rate decreased at higher conversions, depicting a positive order on both p_{CO_2} and p_{H_2} on the rate of reaction at lower values of p_{CO_2} and p_{H_2}. Figure 20 shows the decrease in the rate of reaction with higher partial pressures of H_2O.

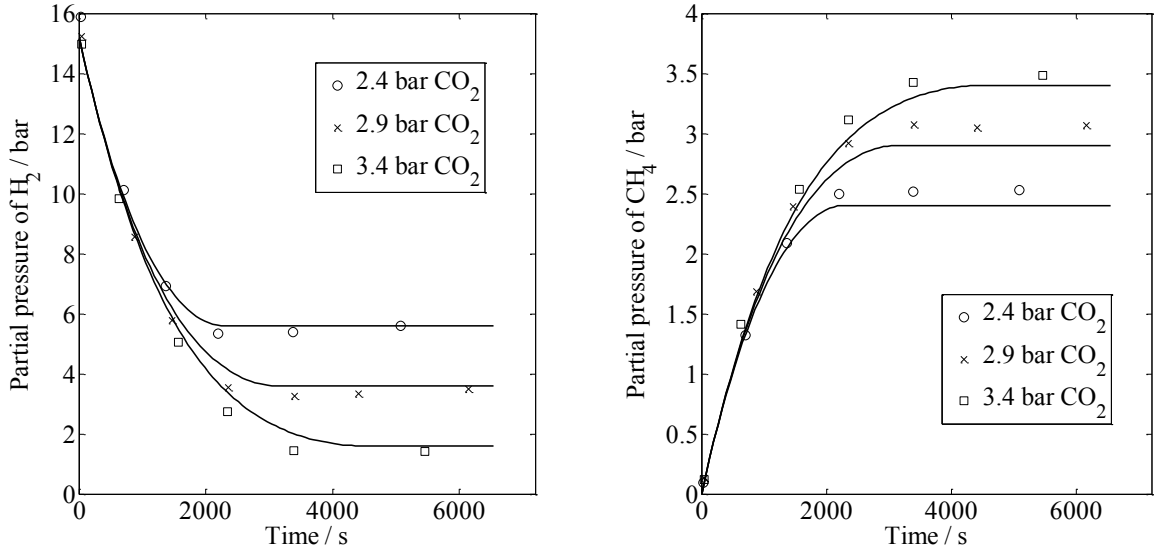

Figure 19. Comparison between the modelling results and the experimental results for different initial partial pressures of CO_2. (a) shows the partial pressure of H_2 with time and (b) the partial pressure of CH_4 with time. $T = 473$ K, $p_{CO_2,0} = 2.4$ bar and $m_{cat} = 5.0$ g. Solid lines are the predictions of Model II and the symbols illustrate the corresponding experimental measurements.

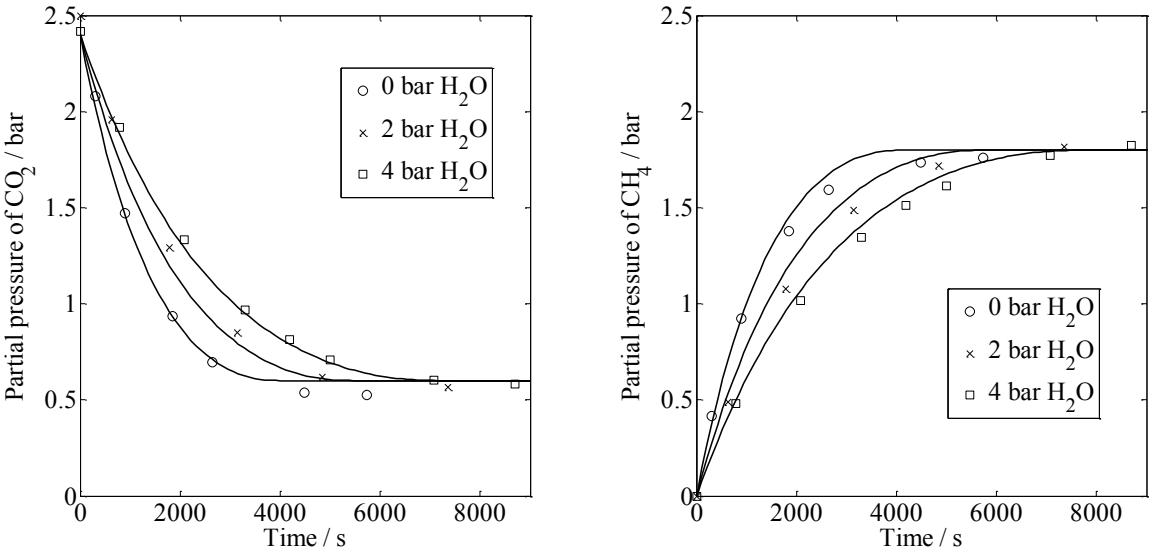

(a) (b)

Figure 20. Comparison between the modelling results and the experimental results for different initial partial pressures of H_2O. (a) shows the partial pressure of H_2 with time and (b) the partial pressure of CH_4 with time. T = 463 K, $p_{CO_2,0}$ = 2.4 bar, $p_{H_2,0}$ = 7.2 bar and m_{cat} = 5.0 g. Solid lines are the predictions of Model II and the symbols illustrate the corresponding experimental measurements.

5. Discussion

It has already been established in Section 4.1.3 that some of the rate expressions proposed by other studies, such as Eqs. (15) and (16), were not suitable for describing the experimental measurements obtained in the present research. Equation (16) was proposed by van Herwijnen *et al.* (1973), who performed the reaction over a similar temperature range to the present investigation. However, the experiments by van Herwijnen *et al.* (1973) only explored p_{CO_2} up to 0.02 bar. They found that the rate followed a first-order dependence on p_{CO_2} at p_{CO2} < 0.004 bar changing to zero order at higher p_{CO_2}, in agreement with the observations in this study. The low threshold of p_{CO_2} when the dependence on p_{CO_2} changed to zero order is likely to the result of a very high ratio of H_2 to CO_2 exceeding 50:1 in their work. While the general trends in the study by van Herwijnen *et al.* (1973) were consistent with those in this study, Eq. (16) did not account for the effects of p_{H_2} and p_{H_2O}. Rate expressions based on a power law, such as Eq. (15), were also found to be unsuitable for the modelling of the different species in the present research. Weatherbee and Bartholomew (1982) also observed that the reaction orders, based on power law expressions, changed significantly with temperature. Hence, the use of power law expressions for CO_2 methanation

is only suitable, at best, over a small range of temperature and partial pressures of reactants and products.

Good agreement between the experimental results and the predictions of Model I was only possible with a very small value of b_I, the adsorption equilibrium of H_2, compared to values reported in the literature (Sehested *et al.*, 2005; Alstrup, 1995; Aparicio, 1997). This contradicts the assumption in Model I that atomic H from the dissociative adsorption of H_2 is one of the most abundant species on the surface of the catalyst. Weatherbee and Bartholomew (1982) also derived an expression similar to Model I, albeit not accounting for H_2O on the surface of the catalyst, and obtained negative parameters. Temperature-programmed desorption studies in the present work performed on the spent catalyst following CO_2 methanation in the Carberry reactor showed no significant evolution of H_2 above 100°C, suggesting that H is not one of the main species on the surface under reaction conditions. Therefore, Model I was rejected on the basis of the evidence from the modelling efforts and experimental measurements.

When the value of b_{II} from Weatherbee and Bartholomew (1982) was used, excellent agreement was obtained between Model II and the experimental results for different p_{CO_2}, p_{H_2}, p_{H_2O} and temperatures. It has already been noted that Model II was based on a similar derivation to that of Eq. (17) but was extended to account for the effect of p_{H_2O}, which cannot be neglected in the present work because the batch operation performed as an integral reactor and the accumulation of H_2O in the reactor was significant. Equation (17) also features an inhibition term involving CO. Weatherbee and Bartholomew (1982) consistently observed a small partial pressure of CO at the outlet of their reactor and attributed it to its being in equilibrium with the adsorbed CO, originating from the dissociative adsorption of CO_2 on the catalyst. However, their reactions were performed at a higher temperature than those described in this work. At 500 K, their lowest temperature, the amount of CO was only 0.003 mol%. Given that the temperature range in the present study was 443 – 483 K, it is likely that p_{CO} was very much smaller because the adsorption of CO_2 is an activated process (Falconer and Zagli, 1980), *viz.* less CO_2 is adsorbed at lower temperatures. This was confirmed by the analysis of the gas samples in the present study, where no CO was detected at all. Furthermore, the thermodynamics of the reaction at such temperatures dictate that p_{CO} is negligible. Therefore, the term involving CO was dropped in the derivation of Model II. This does not contradict the proposed rate mechanism where CO_2 dissociates into CO and O.

The absence of CO is most likely owing to the equilibrium lying heavily on the side of the adsorbed species and the detection limit of the gas chromatograph, approximately 0.05 bar.

The derivation of Model II assumed that CO_2 methanation involves the dissociative adsorption of CO_2 to form surface CO and O. TPD analysis on the spent catalyst following CO_2 methanation, illustrated in Figure 15, showed the evolution of CO_2 and CH_4 from 200 – 350°C, indicating the presence of some carbonaceous species on the catalyst. IR spectra obtained from *in-situ* DRIFTS analysis of the catalyst at 463 K, illustrated in Figure 16, clearly showed the presence of straight and bridged carbonyl groups. The high activity of these groups, evident from the fast decrease in the intensity of their corresponding IR bands when pure H_2 was passed through the catalyst, suggests the involvement of the carbonyl groups in the reaction pathway to form CH_4. The DRIFTS analysis also revealed the presence of formate species, presumably from the hydrogenation of carbonyl and carbonate species. However, the DRIFTS measurements found that formate groups persisted even after 40 minutes under a flow of H_2, indicating that they were bound much more strongly to the surface of the catalyst than the carbonyl groups, which decreased very rapidly. This provides further evidence that while hydrogen-modified groups were tightly bound to the surface, their reactivity is low and so they might not participate in the pathway to form CH_4. These observations are consistent with those of Fujita *et al.* (1993), Jacquemin *et al.* (2010) and Aldana *et al.* (2013), who obtained similar spectra on Ni/SiO_2 and Ni/Al_2O_3 to those observed in this study. Their studies also supported the dissociation of CO_2 followed by the subsequent hydrogenation of adsorbed C species for nickel supported on Al_2O_3 or SiO_2.

Finally, the derived model, with the accompanying parameters for Model II, was compared against additional independent experiments performed in the Carberry reactor. In Figure 21, CO_2 methanation was performed at 463 K with an initial inventory of 2.4 bar CO_2 and 7.2 bar H_2. At 3180 s, additional CO_2 and H_2 were introduced and the composition of the bulk phase of the reactor was analysed periodically. In general, there is good agreement between the results predicted by the model and the measurements obtained from the batch reactor. It is noted that the rate of reaction after the introduction of additional reactants, *viz.* CO_2 and H_2, was predicted to be slightly faster by the model than was the case in practice. This suggests that the inhibition term for H_2O is slightly underestimated in Model II. Nevertheless, there is excellent agreement in Figure 22, where only additional H_2 was introduced at 3780 s. Kinetic expressions proposed by other studies, given in Table 2, were also compared against the experimental results in this study. They consistently predicted a

much faster rate of reaction after the introduction of additional reactants in Figure 21 and 22. This is probably the result of the absence of an inhibition term for H_2O, which limits their accuracy under conditions where p_{H_2O} is high.

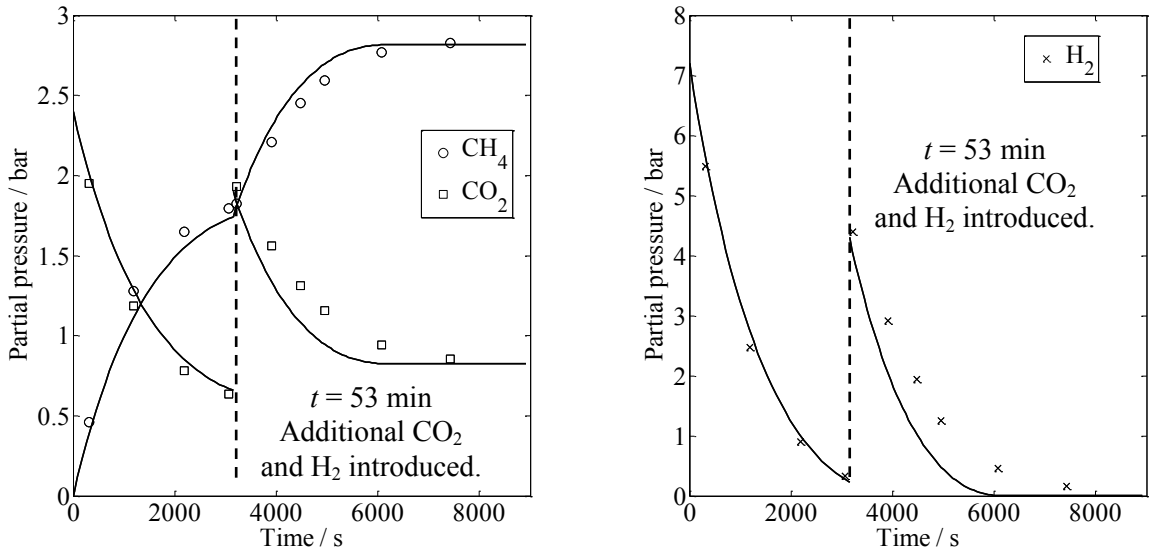

Figure 21. (a) Partial pressure of CO_2 and CH_4 and (b) partial pressure of H_2 versus time. Additional CO_2 and H_2 was introduced in a ratio of 3:1 at t = 3180 s. T = 463 K and m_{cat} = 5.0 g.

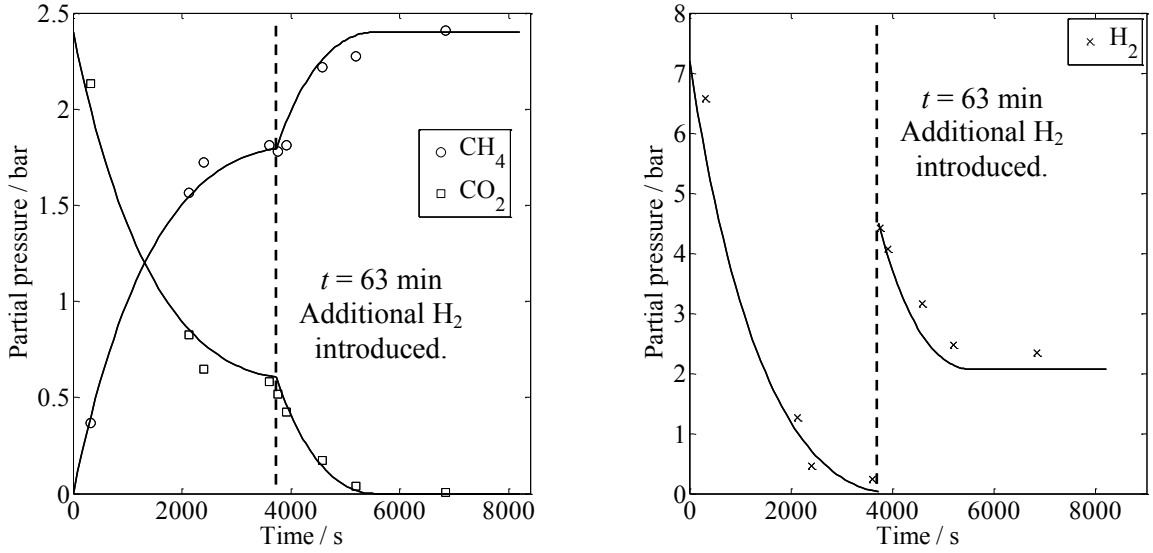

Figure 22. (a) Partial pressure of CO_2 and CH_4 and (b) partial pressure of H_2 versus time. Additional 4.5 bar of H_2 was introduced at t = 3780 s. T = 463 K and m_{cat} = 5.0 g.

6. Conclusions

An investigation of the methanation of CO_2 methanation was performed in a gradientless, spinning-basket reactor at temperatures of 443 – 483 K and pressures of up to 20 bar. The reactor was operated in batch and the composition of its contents was determined periodically. Additional analysis was performed using temperature-programmed studies and DRIFTS analysis in order to probe the surface of the catalyst.

The conclusions were as follows. At low p_{H_2} and p_{CO_2}, the rate increases with the partial pressure of the reactants. At high p_{H_2} and p_{CO_2}, the rate of reaction has a zeroth order relationship with the partial pressure of the reactants. H_2O has a significant inhibitory effect on the rate of CO_2 methanation. Several rate expressions were tested against the experimental measurements and Eq. (12) was found to be the most satisfactory. It assumes a mechanism in which CO_2 dissociates to adsorbed CO and O on the surface of the catalyst. The rate-limiting step was taken to be the dissociation of adsorbed CO and the most abundant species were CO, O and H_2O. The resulting adsorbed carbon on the surface would be further hydrogenated to form CH_4. Temperature-programmed studies of the spent catalyst showed the presence of some carbonaceous species on the catalyst. Their presence was not sufficient to cause any deactivation but were consistent with the dissociation of CO_2 on the surface of the catalyst. The presence of carbonyl groups from *in-situ* DRIFTS analysis is also in agreement with this observation.

Overall, it has been demonstrated that the study of CO_2 methanation in batch has led to experimental measurements consistent with investigations, described in the literature, performed in reactors operated in continuous flow. Furthermore, the validity of different rate expressions could be easily determined over a wide range of partial pressures by using a batch reactor. A convenient method of determining the effect of H_2O on the rate of reaction was discovered and the inhibitory effect of H_2O was quantified.

In terms of further work, the research has indicated that it is possible for nickel-based catalysts with different supporting materials to undergo a different rate mechanism, as suggested by Aldana *et al.* (2013). Therefore, it would be informative to explore the kinetics of such catalysts in the batch reactor in order to determine if proposed rate expressions agree with the proposed rate mechanism. It would also be sensible to explore the impact of temperatures higher than those possible in the Carberry reactor used here, perhaps by using a packed bed reactor with a recycle of gas.

Acknowledgements

JYL was funded by the Cambridge International Scholarship Scheme. The Cambridge Philosophical Society, the Lundgren Research Award and Corpus Christi College are also gratefully thanked for contributing to the support of his PhD studies. We are grateful for the assistance of Dr A.P.E. York, Johnson Matthey Technology Centre, Sonning Common, Reading RG4 9NH, United Kingdom, for his valuable input to this research.

References

Aksoylu, A. E., Akin, A. N., Önsan, Z. İ., Trimm, D. L. (1996). Structure/activity relationships in coprecipitated nickel-alumina catalysts using CO_2 adsorption and methanation. *Applied Catalysis A: General*, **145** (1), 185-193.

Aldana, P. A., Ocampo, F., Kobl, K., Louis, B., Thibault-Starzyk, F., Daturi, M., Bazin, P., Thomas, S., Roger, A. C. (2013). Catalytic CO_2 valorization into CH_4 on Ni-based ceria-zirconia. Reaction mechanism by *operando* IR spectroscopy. *Catalysis Today*, **215**, 201-207.

Alstrup, I. (1995). On the kinetics of CO methanation on nickel surfaces. *Journal of Catalysis*, **151** (1), 216-225.

Aparicio, L. M. (1997). Transient isotopic studies and microkinetic modeling of methane reforming over nickel catalysts. *Journal of Catalysis*, **165** (2), 262-274.

Aresta, M., Dibenedetto, A. (2007). Utilisation of CO_2 as a chemical feedstock: opportunities and challenges. *Dalton Transactions*, **28**, 2975-2992.

Chiang, J. H., Hopper, J. R. (1983). Kinetics of the hydrogenation of carbon dioxide over supported nickel. *Industrial & Engineering Chemistry Product Research and Development*, **22** (2), 225-228.

Du, G., Lim, S., Yang, Y., Wang, C., Pfefferle, L., Haller, G. L. (2007). Methanation of carbon dioxide on Ni-incorporated MCM-41 catalysts: The influence of catalyst pretreatment and study of steady-state reaction. *Journal of Catalysis*, **249** (2), 370-379.

Falconer, J. L., Zağli, A. E. (1980). Adsorption and methanation of carbon dioxide on a nickel/silica catalyst. *Journal of Catalysis*, **62** (2), 280-285.

Fujita, S. I., Nakamura, M., Doi, T., Takezawa, N. (1993). Mechanisms of methanation of carbon dioxide and carbon monoxide over nickel/alumina catalysts. *Applied Catalysis A: General*, **104** (1), 87-100.

Fujita, S., Terunuma, H., Nakamura, M., Takezawa, N. (1991). Mechanisms of methanation of carbon monoxide and carbon dioxide over nickel. *Industrial & Engineering Chemistry Research*, **30** (6), 1146-1151.

Gao, J., Liu, Q., Gu, F., Liu, B., Zhong, Z. and Su. F. (2015). Recent advances in methanation catalysts for the production of synthetic natural gas. *RSC Advances*, **5**, 22759-22776.

Jacquemin, M., Beuls, A., Ruiz, P. (2010). Catalytic production of methane from CO_2 and H_2 at low temperature: Insight on the reaction mechanism. *Catalysis Today*, **157** (1), 462-466.

Kopyscinski, J., Schildhauer, T. J., Biollaz, S. (2010). Production of synthetic natural gas (SNG) from coal and dry biomass–A technology review from 1950 to 2009. *Fuel*, **89** (8), 1763-1783.

Kowalczyk, Z., Stołecki, K., Rarog-Pilecka, W., Miśkiewicz, E., Wilczkowska, E., Karpiński, Z. (2008). Supported ruthenium catalysts for selective methanation of carbon oxides at very low CO_x/H_2 ratios. *Applied Catalysis A: General*, **342** (1), 35-39.

Levenspiel, O. (1972). Chemical Reaction Engineering, Wiley.

Liu, J., Li, C., Wang, F., He, S., Chen, H., Zhao, Y., Duan, X. (2013). Enhanced low-temperature activity of CO_2 methanation over highly-dispersed Ni/TiO 2 catalyst. *Catalysis Science &*

Technology, **3** (10), 2627-2633.

Ma, J., Sun, N., Zhang, X., Zhao, N., Xiao, F., Wei, W., Sun, Y. (2009). A short review of catalysis for CO_2 conversion. *Catalysis Today*, **148** (3), 221-231.

Marwood, M., Doepper, R., Renken, A. (1997). In-situ surface and gas phase analysis for kinetic studies under transient conditions The catalytic hydrogenation of CO_2. *Applied Catalysis A: General*, **151** (1), 223-246.

Porosoff, M.D. and Chen, J.G. (2013). Trends in the catalytic reduction of CO_2 by hydrogen over supported monometallic and bimetallic catalysts. *Journal of Catalysis*, **301**, 30-37.

Riedel, T., Schulz, H., Schaub, G., Jun, K. W., Hwang, J. S., Lee, K. W. (2003). Fischer–Tropsch on iron with H_2/CO and H_2/CO_2 as synthesis gases: the episodes of formation of the Fischer–Tropsch regime and construction of the catalyst. *Topics in Catalysis*, **26** (1-4), 41-54.

Sehested, J., Dahl, S., Jacobsen, J., Rostrup-Nielsen, J. R. (2005). Methanation of CO over nickel: Mechanism and kinetics at high H_2/CO ratios. *The Journal of Physical Chemistry B*. **109** (6), 2432-2438.

Van Herwijnen, T., Van Doesburg, H., & De Jong, W. A. (1973). Kinetics of the methanation of CO and CO_2 on a nickel catalyst. *Journal of Catalysis*, **28** (3), 391-402.

Weatherbee, G. D., Bartholomew, C. H. (1982). Hydrogenation of CO_2 on group VIII metals: II. Kinetics and mechanism of CO_2 hydrogenation on nickel. *Journal of Catalysis*, **77** (2), 460-472.

Weisz, P. B., Prater, C. D. (1954). Interpretation of measurements in experimental catalysis. *Advances in Catalysis and Related Subjects*, **6**, 143.

Young, J. B., Todd, B. (2005) Modelling of multi-component gas flows in capillaries and porous solids. *International Journal of Heat and Mass Transfer*, **48** (25-26), 5338-5353.

Xu, J. & Froment, G.F. (1989). Methane steam reforming, methanation and water-gas shift: 1. intrinsic kinetics. *A.I.Ch.E.J.*, **35**, 88-96.

Zağli, E., Falconer, J. L. (1981). Carbon dioxide adsorption and methanation on ruthenium. *Journal of Catalysis*, **69** (1), 1-8.

Zhang, Y., Jacobs, G., Sparks, D. E., Dry, M. E., Davis, B. H. (2002). CO and CO_2 hydrogenation study on supported cobalt Fischer–Tropsch synthesis catalysts. *Catalysis Today*, **71** (3), 411-418.